Geo-information Science and Remote Sensing

Thesis Report GIRS-2018-13

IDENTIFICATION OF URBAN PARAMETERS IN TWO LATIN-AMERICAN CITIES USING MID-RESOLUTION OPEN REMOTE SENSING DATA

Bettina Felten

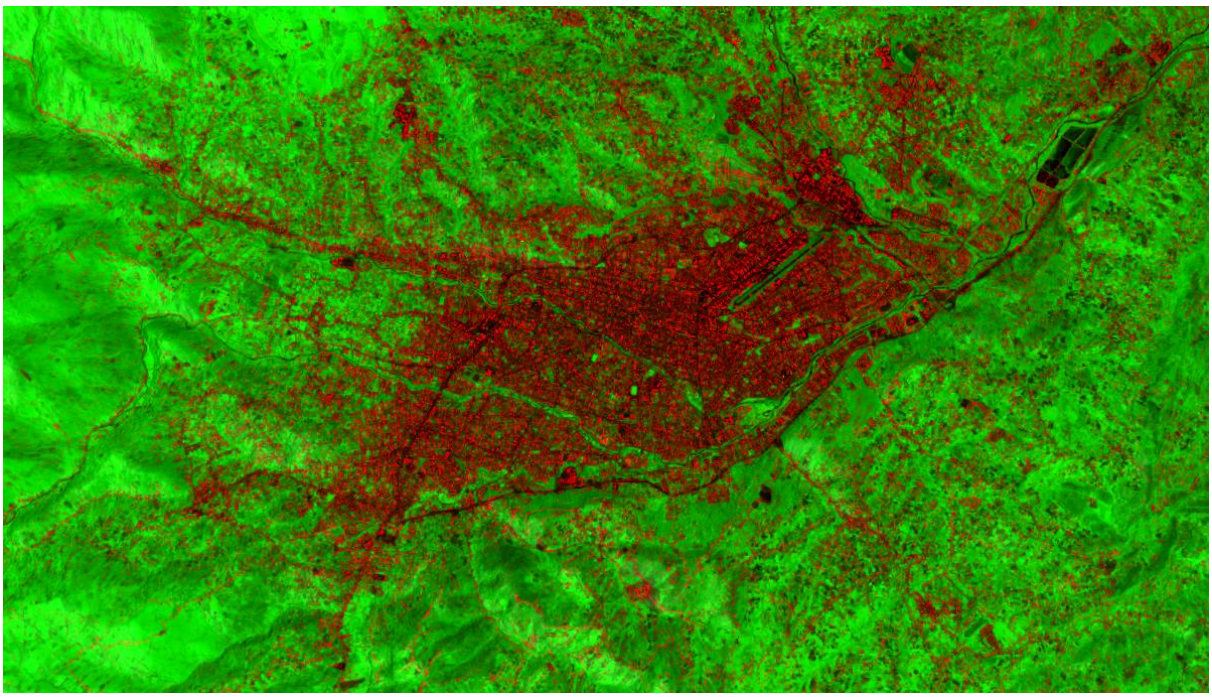

25.04.2018

WAGENINGEN
UNIVERSITY & RESEARCH

Identification of Urban Parameters in Two Latin-American Cities Using Mid-Resolution Open Remote Sensing Data

Bettina Felten

Registration number 920611238040

Supervisors:

Daniel Orellana
Jan Clevers

A thesis submitted in partial fulfilment of the degree of Master of Science
at Wageningen University and Research Centre,
The Netherlands.

25.04.2018
Wageningen, The Netherlands

Thesis code number: GRS-80436
Thesis Report: GIRS-2015 -13
Wageningen University and Research Centre
Laboratory of Geo-Information Science and Remote Sensing

Title image: Composite of Morphological Building Index (red) and Normalized Difference Vegetation Index (green) derived from PlanetScope 2 data acquired on the 2017-09-21 with digital elevation model, Cuenca.

Abstract

Urban form or texture can influence transportation choices in cities. In previous works, it was found that parameters of urban form such as density, connectivity, roughness, and compactness can be linked to transportation choices. Furthermore, types of urban texture can also influence transportation choices. In Andean cities such as Cuenca and Quito (Ecuador), data about urban land cover is often incomplete or outdated. Therefore, the suitability of mid- and high-resolution remote sensing data, i.e. Sentinel 2 (ESA) and PlanetScope 2 (Planet Inc.), for the extraction of urban parameters linked to transportation choices was investigated. A method for urban land cover classification based on multispectral and morphological indices as well as shape metrics was developed. The method produced an accuracy of 0.81 with a Cohen's Kappa coefficient of 0.67 with PlanetScope 2 data and an accuracy of 0.77 with a Cohen's Kappa of 0.57 with Sentinel 2 data, outperforming spectral mixture analysis, random forest classification, and object-based image analysis. Density, connectivity, and compactness were derived from the land cover classification and roughness from the JAXA ALOS open DEM. Additionally, the Normalized Difference Vegetation Index (NDVI) and Morphological Building Index (MB) were derived from remote sensing images. The link between these urban parameters and types of urban texture was investigated through a random forest model attempting to predict types of texture from urban parameters. Types of texture could be predicted with a classification accuracy of 0.79. Density and connectivity had the greatest influence on model accuracy.

Contents

List of Figures

List of Tables

1 Introduction

1.1 Context and Background

The research group “Llactalab – Sustainable Cities” of the University of Cuenca, Ecuador, initiated a research project on the relationship between urban form, modes of transportation, technological innovation, alternative energy and socio-economic development with the final objective of decreasing traveling and increasing the efficiency of transportation systems through sustainable urban planning in Quito and Cuenca (Hermida et al., 2017). To achieve this, Llactalab will investigate the link between urban structure and transportation choices. An important pre-condition for the project is the identification of types of urban form in the research areas. In Andean cities such as Quito and Cuenca (s. Figure 1), exact and current data about urban structures are not always available. Cities change at a high rate and often in an informal way unregistered by authorities. Mid-resolution open remote sensing data are an extensive and cost-efficient source of information. Due to their wide temporal and spatial coverage, they are useful to analyze and compare structures of urban areas (Balstad-Miller and Small, 2003). According to Weng (2012), the term refers to data with a spatial resolution of 10-100 m.
Due to their disperse structure and rapid growth (Inostroza et al., 2013), Latin-American cities induce inhabitants to extensively use individual cars, leading to high consumption of fossil fuels as well as large emissions. Quito is the capital and second largest city of Ecuador with a population of about 2.3 million in 2010. Cuenca had about 500,000 inhabitants in 2010 (Instituto Nacional de Estadística y Censos, 2010). Quito is located very close to the equator and Cuenca at about 2.9 $^{\circ}$ S (s. Figure 1). Both cities are located in mountainous areas, at altitudes of around 2,800 and 2,400 m, respectively. High altitudes can increase the effects of air pollution due to a greater frequency of inversion (Brachtl et al., 2009).

1.2 Problem definition

The starting point of the research is a need to classify urban forms based on parameters that might influence transportation choices in view of low data availability. Urban form is often characterized as a combination of parameters or metrics, i.e. quantifiable characteristics (Song et al., 2013). The discipline that attempts a conceptual analysis and description of urban structures as a human habitat is known as urban morphology (Vernez-Moudon, 1997). Cities are described as an agglomeration of basic structures like buildings, streets or gardens and exist in a spatial as well as temporal context (ibid). Urban texture can be defined as recurring patterns in the urban landscape. A comprehensive typology is proposed by Wheeler (2015) who defines types of built landscapes as "(...) an area of consistent form at a neighborhood scale, often 1 square km or greater" (Wheeler, 2015). His urban texture analysis is based mainly on street, block, and parcel patterns which are extracted visually from high resolution images (ibid).
Researchers identify a number of parameters of urban morphology or texture, depending

Figure 1: Research area: The cities Quito (red) and Cuenca (blue). Map data ©2015 Google. Projection: WGS 1984. Coordinates: Longitude / latitude.

on the scale and objective of their research. In the following paragraphs, parameters that can be extracted from remote sensing data and that were found to influence transportation choices are discussed. These parameters are:

- Degree of urbanization: Density of built structures
- Size and overall structure (mono- or polycentric) of the city
- Connectivity: Number of intersections and street density
- Roughness
- Compactness

Density (or degree of urbanization, urban-rural gradient) can be quantified using the ratio of impervious surfaces at a pixel or sub-pixel scale (Weng, 2012). The overall shape of a city also plays a role; Kang et al. (2012) found that residents of large and irregular shaped cities tend to travel more during their daily routine. Bertaud et al. (2009) come to the same conclusion, adding that high density and monocentric cities have a lower percentage of individual motorized transport. Moreover, minibuses and individual cars are more effective if both the origins and destinations of commuters are disperse (ibid).
Connectivity describes the amount of reachable areas of a certain type from one area and originates from spatial ecology (Calabrese and Fagan, 2004; Bierwagen, 2007), but is also applicable to human movements in urban areas (Kang et al., 2012). The number of

intersections per area is an important indicator of connectivity. It also has a direct influence on travel choice behavior; travel speed is lower in areas with many intersections and the traversed distance can be perceived to be longer (Sadalla and Staplin, 1980). Furthermore, users of more connected streets in New Zealand were found to be more likely to engage in travel-related physical activity when commuting to their workplace (Badland et al., 2008). Beside the number of intersections, street density is another indicator of connectivity (Song et al., 2013). Surface roughness describes the deviation of elevations from an ideal (smooth) surface. It can have two impacts on transportation choices; on the one hand, roughness has an important impact on wind speed and ventilation (Ng et al., 2011), thus influencing the possibilities of physical movement. On the other hand, a high roughness at the scales of both landscape and streets can make cycling and walking less attractive for residents and increases the amount of energy needed for all kinds of transport. Compactness can be an indicator of the development of cities. Residents of compact cities tend to move less than residents of less compact ones (Kang et al., 2012). Compactness can be defined as the ratio between the perimeter and the area of a shape, a circle being the most compact shape possible (ibid). An area is compact if it contains mostly closed shapes. Compactness of a city implies close proximity of residences and services, including the workplace.

We assume that types of urban form can be identified through an analysis of the combinations of these and / or similar parameters of urban morphology. To achieve this, parameters must be (1) extractable from the available data, (2) sufficiently variable and meaningful to distinguish between areas, (3) applicable to different cities, and (4) not highly correlated with each other (Song et al., 2013). As few parameters as possible without substantial information loss should be used (ibid).

The methods used to analyze urban structure using geographic information systems (GIS) found in recent literature are diverse. Examples based on mid-resolution remote sensing data include Spectral Mixture Analysis (SMA), Artificial Neural Networks (ANN), Classification and Regression Tree (CART), and object-based approaches (Weng, 2012; Sugg et al., 2014; Small, 2002). Small (2002) found that 90 % of the variation within cities can be described as linear combinations of three endmembers, i.e. high albedo, dark, and vegetation based on Landsat 7 data. To adequately characterize infrastructure, spatial resolutions higher than 10 m were found to be necessary in most cities (Balstad-Miller and Small, 2003). To quantify roughness at a neighborhood scale, a digital elevation or building model are required.

Mid-resolution remote sensing data have successfully been used to derive characteristics of cities at a regional scale. A spatial resolution larger than 10 m is usually not sufficient to analyze individual built structures or infrastructure at a local scale. Road extraction has mainly been applied to high resolution data (Wang et al., 2016; Benediktsson et al., 2003; Peteri and Ranchin, 2004), often in combination with other data sources such as LiDAR or high resolution elevation data (Haala and Brenner, 1999). However, through spectral unmixing, linear features at a sub-pixel level could be extracted from Sentinel 2 data (Radoux et al., 2016). Furthermore, transportation choices of commuters in particular are

also linked to the overall structure of the urban environment (Kang et al., 2012).
Due to a lack of high-resolution remote sensing or up-to-date cadaster data in Andean cities, the exploration of open mid-resolution remote sensing data is an important step towards the classification of urban morphology and texture as well as the investigation of its link to transportation choices.

1.3 Research objectives and research questions

The objective of the M.Sc. thesis is to explore the potential of mid-resolution remote sensing data to classify urban textures with regard to parameters of urban morphology at a district-wide scale for the cities of Cuenca and Quito.

Research questions:

1. Which parameters of urban morphology can be extracted from mid-resolution open remote sensing data using open software?
2. Which analytic methods and techniques are suitable to classify remote sensing images according to these parameters?
3. What is the added value of PlanetScope 2 data as an example of commercial high-resolution remote sensing imagery?

The results of the thesis will be used by the research group Llactalab to investigate the relationship between urban form and transportation choices in Cuenca and Quito. Thus, the main output is a classification of both cities with regard to relevant parameters of urban morphology. To insure reliability, uncertainties were quantified as far as possible at every step. Furthermore, methods developed during the thesis work may be applied to other Andean cities in the future. The added value of the thesis work to the research of Llactalab is (1) comprehensive information about the structure of two current research areas, i.e. Cuenca and Quito, (2) a reproducible method for the classification of urban areas based on mid-resolution open remote sensing data, and (3) conclusions about the use of open remote sensing data for the classification of parameters of urban morphology and texture in two Latin American cities compared to commercial high-resolution data.

2 Methods

2.1 Data

2.1.1 Land Cover Classification and Parameter Extraction

Most of the urban parameters enumerated in chapter 1.2, i.e. **density**, **connectivity**, and **compactness**, can be computed based on an urban land cover map. Land cover was classified using mid- and high-resolution remote sensing data. An important source of mid-resolution open remote sensing data is the Copernicus mission of the European Space Agency (ESA). Sentinel 2, the Copernicus satellite carrying sensors that cover the optical and infrared spectra, orbits the earth since 2015 and produces images with a spatial resolution of up to 10 m (s. Table 1). The added value of commercial high-resolution imagery was explored using an ortho-rectified Top of Atmosphere (level 3B) data product (s. Table 1) from the company Planet acquired by sensors of the PlanetScope 2 constellation (Planet Lab Inc., 2017). PlanetScope 2 consists of a flock of nano-satellites that orbit the earth at an altitude of 475 km (ibid). Planet launched the first flock in 2014. Data are made available for research without cost by the company Planet.
In addition to multispectral remote sensing data, Sentinel 1 RADAR imagery was used to investigate whether additional information about image texture can improve land cover classification. Image texture refers to surface characteristics which can be derived from RADAR images (s. Chapter 2.2.3). Sentinel 1 is a constellation of two satellites with C-SAR sensors which orbit the earth since 2013. Being active systems, they provide mid- and high- resolution data regardless of weather conditions, passing over the same area every 1-3 days (European Space Agency (ESA), 2017b). The data used for image texture computation are high-resolution ground-range detected (GRD) level 1 products in Interferometric Wide swath (IW) mode. The resolution is 20x22 m and the equivalent number of looks (ENL) 4.9 (ibid).
Roughness was computed using the Japan Aerospace Exploration Agency's ALOS DEM with a spatial resolution of 30 m based on images acquired between 2006 and 2011 (Japan Aerospace Exploration Agency, 2017).

2.1.2 Validation and Reference Data

Aerial photography is provided by the Ecuadorian geo-information platform sigtierras (Ministerio de Agricultura, Ganadería, Acuacultura y Pesca, 2017). Another validation dataset is a detailed vector layer showing building blocks in Cuenca which was digitized manually by volunteers for the Open Street Map (OSM) project. However, these data do not cover informal settlements and urban sprawl around the cities and are partly outdated. Aerial imagery of Ecuadorian cities was last acquired in 2011 and is therefore considered to be outdated, too. Additionally, the developed method should be applicable to other Andean cities where no aerial photography and OSM data are available. Therefore, OSM data and

Table 1: Sources for optical and multispectral remote sensing data (European Space Agency (ESA), 2017a; Planet Lab Inc., 2017)

Data source	Spatial resolution	Bands	Spectral resolution (µm)	Return time
Sentinel 2	10 m	B2	0.448 - 0.546	10 days
		B3	0.538 - 0.582	
		B4	0.646 - 0.684	
		B8	0.763 - 0.908	
	20 m	B5	0.694 - 0.713	
		B6	0.731 - 0.749	
		B7	0.769 - 0.797	
		B8a	0.848 - 0.881	
		B11	1.542 - 1.685	
		B12	2.081 - 2.323	
	60 m	B1	0.430 - 0.457	
		B9	0.932 - 0.958	
		B10	1.336 - 1.411	
PlanetScope 2	3.125 m	Red	0.630 - 0.714	1 day
		Green	0.515 - 0.610	
		Blue	0.424 - 0.478	
		NIR	0.770 - 0.900	

aerial photography were only used for validation.
To investigate the relationship between urban parameters and urban texture, a manual classification of urban texture according to the methods of Wheeler (2015) in Cuenca implemented by two students of the University of Cuenca was used as a reference (Cobo and Neira, 2018) (s. Figure 2).

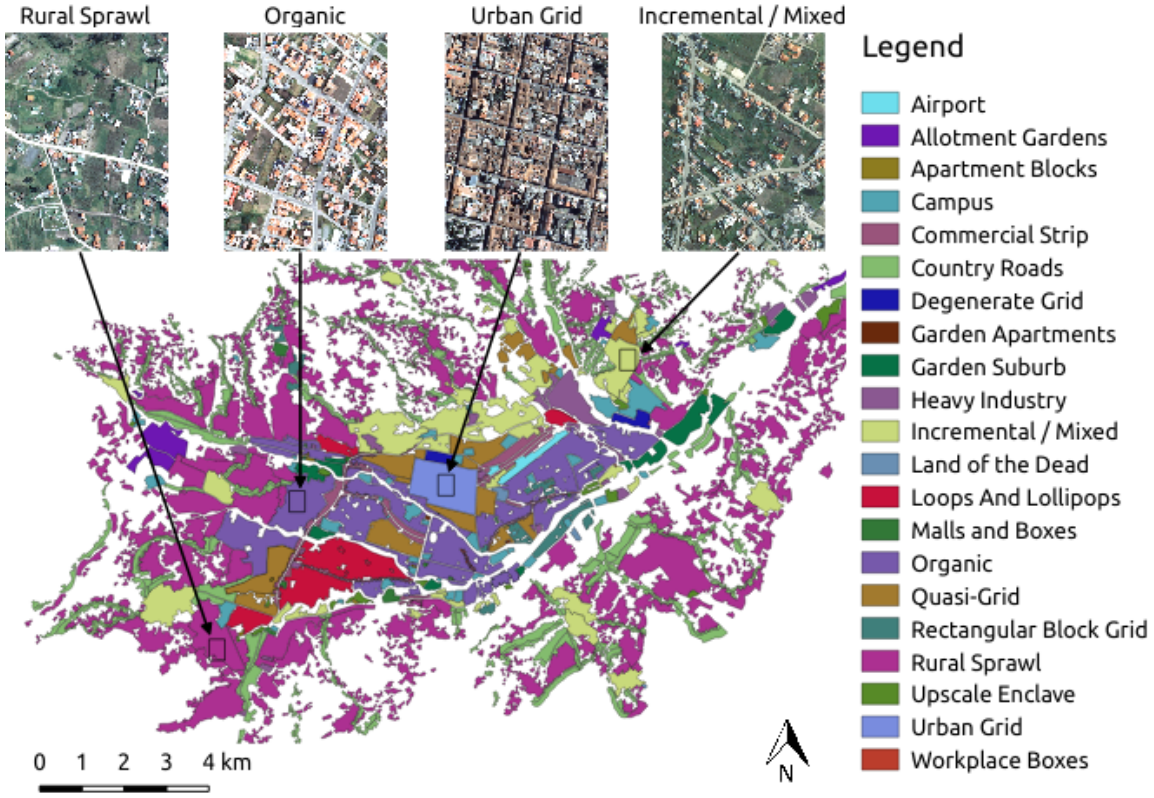

Figure 2: Urban texture in Cuenca and its area of influence, classified according to Wheeler (2015). With permission from Carolina Neira and Daniela Cobo.

2.2 Workflow

2.2.1 Overview

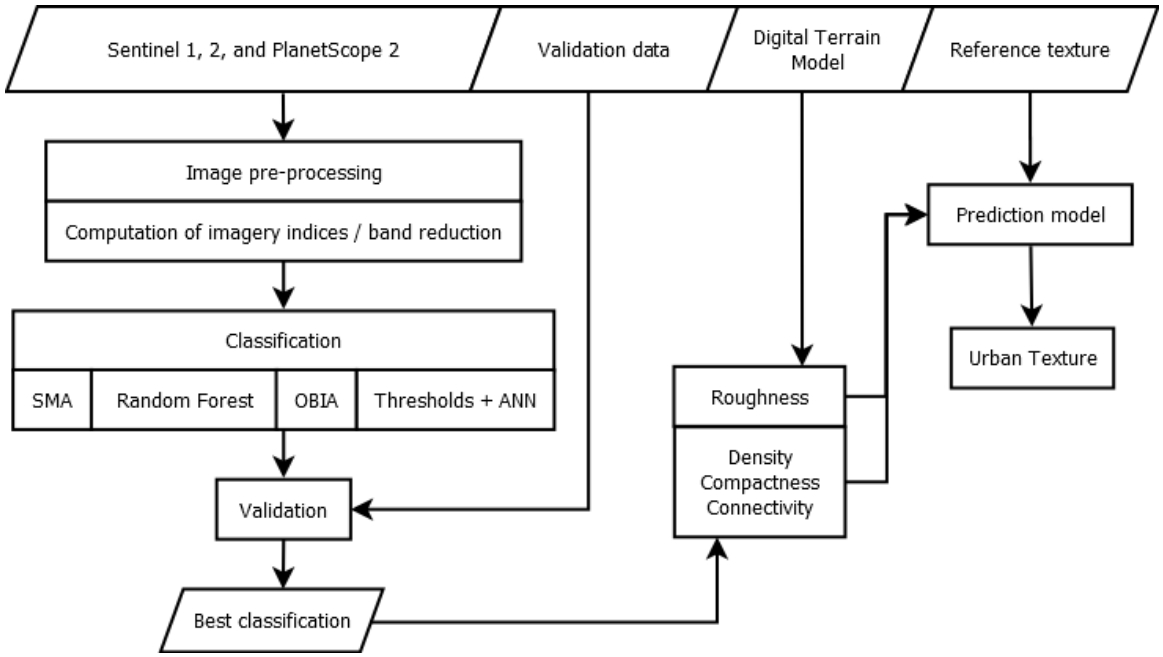

Figure 3: Workflow.

As described above (s. Chapters 1.2, 1.3), the main goal of the research is to gain understanding about urban form in two Andean cities in Ecuador based on mid- and high-resolution remote sensing data. To achieve this, several analysis steps were developed (s. Figure 3). The first step after data acquisition (s. Chapter 2.1) and pre-processing (s. Chapter 2.2.2) is image classification. To derive urban parameters like density and connectivity, buildings and roads need to be identified with high certainty. Therefore, different classification techniques were compared with regard to their ability to (1) separate built-up areas from other land cover types, and (2) separate the main urban classes buildings and roads (s. Chapter 2.2.4). The methods tested include pixel, sub-pixel, and object based image analysis (OBIA) techniques. The assumption of pixel-based classification techniques is that each pixel can be assigned to a certain class. Sub-pixel classification techniques, on the other hand, take mixed pixels into account, meaning that the spectral signature of one pixel can be composed of several classes combined in a linear or non-linear way. With OBIA, not only individual pixels, but also their spatial context is taken into account. Thus, two pixels with the same spectral signature may be classified differently according to the characteristics of the surrounding pixels. Pixel-based image classification with a random forest model was used as a baseline. After the best classification technique was identified, urban parameters based on land cover classification, i.e. density, compact-

ness, and connectivity (s. Chapter 1.2) were derived. Roughness was computed based on elevation data. To investigate the correlation between these parameters and urban form, a reference dataset (s. Chapter 2.1 and Figure 2) was used. The analysis was implemented in open source software, specifically QGIS 5.1, GRASS GIS 7.0, R Studio with R 3.4.1, the Orfeo Toolbox (OTB) 6.4.0, and the Sentinel 1 and 2 processing toolboxes provided by ESA with SNAP 5.0.

2.2.2 Pre-Processing

Only images acquired between August 2016 and September 2017 (Cuenca) and between September and December 2017 (Quito) (s. Table 2) with little atmospheric disturbance were used. To improve the reliability of analysis results, basic atmospheric correction with the sen2cor tool (Mueller-Wilm et al., 2018) was applied to Sentinel 2 imagery and clouds and cloud shadows were masked using IDEPIX in SNAP 5.0 (Brockmann Consult GmbH, 2017). Furthermore, the 'super-resolution' tool for SNAP 5.0 (Brodu, 2016) was applied to sharpen all bands to a resolution of 10 m. Different images acquired during the same year were stitched to minimize cloud cover. First, each of the images was masked and then, the no-data areas in one image were filled with values from the other images. Pixels masked in all images were filled with values from the image with least cloud cover as it was assumed that they represent bright areas misclassified as clouds. Thus, the resulting image may contain some clouds if areas with continuous cloud cover throughout the year exist in the area of interest, which applied to the case of Cuenca.
PlanetScope 2 data were combined through the mosaic tool from the R raster library and cropped to the area of interest. Due to the high temporal resolution, cloud-free images of both research areas could be acquired.
Sentinel 1 imagery was pre-processed using the respective toolbox in SNAP 5.0. The calibrate, multilook and terrain correction tools were applied to obtain pixels of equal size and correct location in the projection system used in this research (WGS 84 / UTM Zone 17 S). Speckle removal was not applied as it leads to information loss concerning image texture.

2.2.3 Computation of Imagery Indices / Band Reduction

Several indices, i.e. New Built Index (NBI) (Waqar et al., 2012), Normalized Difference Vegetation Index (NDVI), and Mc Feeters' Normalized Difference Water Index (NDWI) (McFeeters, 1996), were calculated to highlight certain types of land cover (s. Equations 1, 2, 3). Buildings were highlighted using the Morphological Building Index (MBI) proposed by Huang et al. (2014). This index is calculated as the white tophat of the brightness with brightness being defined as the maximum value in the visible spectrum (red, green, blue bands) (Huang et al., 2014). The white tophat transform highlights bright areas smaller than a structuring element. A disk with a radius of eight pixels for PlanetScope 2 images and two pixels for Sentinel 2 images were used. Another possibility to separate build-

ings from other built-up areas is the redness index (RI) which highlights red brick roofs (s. Equation 4). For image segmentation, edges were enhanced with the Touzi filter. The Touzi filter is an adaptive edge enhancement operation often used for SAR images as it can deal with speckle or noise by calculating means on both sides of the edge. The filter is multi-directional as it retains the maximum response of the four main image directions. The result is similar to a Sobel filtered image, but somewhat smoother.
To compute image texture metrics from pre-processed Sentinel 1 C-SAR imagery, the first principle component of both polarisation modes - VH and VV - was computed to obtain a single image for texture computation. Then, the Gray-Level Co-occurrence Matrix (GLCM) was computed based on this image. Image texture is a description of the relationships between neighboring pixels. The co-occurrence matrix shows the occurrence of combinations of pixel values in neighboring pixels. On this basis, image texture metrics can be calculated. The metrics chosen for this research are contrast, correlation, energy, and homogeneity. Contrast describes the difference within value pairs; correlation the frequency of occurrrence of each value pair; energy is a measure of orderliness within a window, high energy meaning a great variety of value pairs; homogeneity describes the inverse of contrast weights.

Table 2: Overview on input data.

	Sensor	Acquisition date
Cuenca	PlanetScope 2	2017-09-21
	Sentinel 2	2016-08-12
		2017-03-18
		2017-04-27
		2017-05-17
		2017-06-06
		2017-07-16
	Sentinel 1	2017-09-08
Quito	PlanetScope 2	2017-09-19
		2017-09-20
	Sentinel 2	2017-12-13

$$NBI = \frac{Green * NIR}{Red} \tag{1}$$

$$NDVI = \frac{NIR - Red}{NIR + Red} \tag{2}$$

$$NDWI = \frac{Green - NIR}{Green + NIR} \tag{3}$$

$$RI = \frac{Red - Green}{Red + Green} \tag{4}$$

2.2.4 Land Cover Classification

2.2.4.1 Random Forest

Random forest (RF) classification was implemented in R with the 'randomForest' library. Random forest is a supervised classification technique based on a decision-tree model and generally outperforms classic maximum likelihood classification (Kulkarni and Lowe, 2016). 500 trees and five training areas per class were used.

2.2.4.2 Spectral Mixture Analysis

Spectral Mixture Analysis (SMA) with six endmembers (vegetation, soil, buildings with red brick roofs, buildings with gray / light roofs, asphalt and water) represents sub-pixel classification. Pure endmember pixels were identified based on aerial photography and high resolution satellite imagery from Google (©2015 Google). Furthermore, endmembers of the main classes of interest - i.e. buildings and asphalt - were compared to datasets from the USGS spectral library (U.S. Department of the Interior - U.S. Geological Survey, 2017) (s. also Appendix A). The points used are located in areas of at least 20x20 metres of the same class to avoid mixed pixels in both PlanetScope 2 and Sentinel 2 images. Furthermore, the separability of the spectral signatures was verified by checking the location of each class in a feature space of the first two principal components of the images. For SMA computation, the respective tool from the Orfeo toolbox was used. Unfortunately, only linear models appear to be implemented in open software today. SMA is a 'soft' classification technique as pixels are not assigned a specific class. However, a definite ('hard') classification can be achieved through thresholding or by assigning the class with maximum probability to each pixel. The second approach was applied as it is more objective and ensures greater comparability of the results.

2.2.4.3 Object-Based Image Analysis

OBIA consists of two main steps, image segmentation and feature classification. The following eight datasets comprised of different combinations of the pre-processed input data and indices were prepared and tested with five segmentation algorithms available in open source software. Image segmentation using the MBI or a combination of the MBI and spectral bands was attempted with the region growing and watershed algorithms.

1. Sentinel 2

2. Sentinel 2 and image texture metrics (contrast, correlation, energy, homogeneity) derived from Sentinel 1, stacked
3. NDVI, NDBI, NDWI, contrast, correlation, energy, homogeneity (band reduced Sentinel 1 + 2)
4. PlanetScope 2
5. Sentinel 2 pansharpened using PlanetScope 2
6. Band reduced Sentinel 1 + 2 pansharpened using PlanetScope 2
7. Sentinel 2 with Touzi edge enhanced Sentinel 2 and the NDVI as additional bands
8. PlanetScope 2 with Touzi edge enhanced PlanetScope 2 and the NDVI as additional bands

The segmentation algorithms were chosen to cover the main state-of-the art segmentation algorithms derived from literature. Plus, they all take raster stacks as input, perform relatively fast on a machine with intermediate capacities, and can be implemented in Python.

1. Mean shift segmentation (OTB)
2. Morphological-based segmentation (OTB)
3. Watershed segmentation (OTB)
4. Hierarchical Region Growing (GRASS GIS)
5. Shepherd segmentation (based on k-means clustering) (RSGISLIB)

Mean shift segmentation is a clustering technique which is based on the mean values within a kernel. It starts by calculating the mean within each of the kernels in a feature space. With each iteration, the kernel 'shifts' so that the mean value equals the median value. Overlapping kernels are merged. This means that the number of resulting clusters is not predefined, but depends on the original kernel size. Morphological-based segmentation as implemented in the Orfeo Toolbox is based on a series of operations of mathematical morphology according to Pesaresi and Benediktsson (2001). The input image is classified into three classes: Concave, convex, and flat. Morphological-based segmentation is especially well suited for very high-resolution images as it does not rely on edge detection and is therefore more likely to preserve heterogeneous and nested shapes (Pesaresi and Benediktsson, 2001). The watershed algorithm, on the other hand, strongly relies on edge detection. Pixel values are interpreted as elevation in a terrain model and the watershed algorithm works like a sink filling tool, thus detecting areas between 'value ridges'. Hierarchical region growing starts by over-segmentation of the image, viewing almost each pixel as an object. Then, neighbouring pixels are merged if they do not exceed a certain similarity threshold. Thus, hierarchical region growing has the advantage that it segments the image independent of scale. K-means segmentation according to Shepherd (Clewley et al., 2014) assigns pixels to the nearest cluster centre, then gradually eliminates

small clusters by merging them with nearest neighbors.
The forty resulting vector layers were visually evaluated to select the best combinations of data and segmentation techniques. Results were ordered in three categories; results in which segments do not in any way correspond to the input image (e.g., there is only one segment in the output); segments correspond to the input image, but no features are recognizable; and segmentation results where at least some characteristic features are visually recognizable with basic knowledge of the area of interest.
For feature classification, the vector classification tool based on an artificial neural network implemented in OTB was then applied to those results which allowed an intuitive visual interpretation of distinctive objects with a basic knowledge of the research area and neither lacked detail nor presented signs of over-segmentation. Beside spectral information, the size and circumference of features were taken into account for classification. The polygons were then dissolved by the resulting class attribute.

2.2.4.4 Thresholding and ANN

The last classification technique used is a workflow based on thresholding with indices that describe different properties of urban and non-urban features as well as shape metrics. First, objects with a high MBI were separated. These are bright, small objects, mainly buildings. In Cuenca and Quito, roads often consist of a bright material, thus, most road features could also be selected. To separate buildings from roads, the Redness Index (RI) (s. Equation 4) was applied as most buildings in Cuenca appear to have a red brick tile roof. Then, very dark small features were selected by applying a threshold on a black tophat image derived from the brightness index with a structuring element half the size of the one used for the white tophat operation. Black tophat transform is the reverse of white tophat transform and highlights small objects with a low brightness compared to their surroundings. This step separates small shadowy roads as well as small bodies of water. The NDVI was used to separate vegetated areas from the other objects, and the NDWI to separate shadow and water as far as possible. Next, the resulting image was vectorized. Then, the shape metrics compactness, perforation, elongation (s. Chapter 2.2.6), and area were calculated. The mean values of NDVI, Redness Index, and NDWI were also assigned to each polygon. Then, 5-12 training areas representing each of the four classes building, road, vegetation, and water were selected. The polygons were classified using the Vector Classifier tool from the Orfeo toolbox based on an ANN.

2.2.5 Validation

The classification results were validated using a random sample approach based on aerial photography and Google Earth basemaps (©2015 Google). To determine the number of random samples, the following formula according to Foody (2009) and Congalton & Green

(2009) was applied (s. Equation 5).

$$n = \frac{z_{\alpha/2}^2 * P(1-P)}{h^2} \tag{5}$$

where, P is an initial guess for the population proportion (overall accuracy), h the half width of the desired confidence interval around P and $z_{\alpha/2}$ the critical value of the normal distribution for the two-tailed significance level α.

In our research, $P = 80\%$, $h = 5\%$ and $\alpha = 0.05$, i.e. $(1.96^2 * 0.8 * 0.2)/0.05^2 = 246$ were used. The same validation dataset was used to validate all classification results to ensure comparability.

2.2.6 Urban Parameters

Next, the urban parameters listed in Chapter 1.2 were computed. The average of each parameter was calculated for cells of 100x100 m. The following terrain roughness metric was applied to the DTM in a 3x3 pixels window (s. Equation 6).

$$Roughness = \sigma(\frac{Meanelevation - Elevation}{Range}) \tag{6}$$

Density was quantified by counting the number of polygons classified as urban, i.e. buildings or asphalt, which overlap with each cell of the grid, and the urban area per cell. Compactness was computed as the area of a feature divided by the area of its smallest enclosing circle. Furthermore, an elongation and perforation index were computed; elongation is the quotient of the area of the intersection of a feature and a circle with the same area as the feature and the union of this feature and circle, perforation is the area of holes in a polygon divided by the total area of the polygon (Wentz, 2000). The mean roughness and compactness were computed for each cell. Mean compactness refers to the sum of the compactness indices of all features overlapping a cell divided by the number of features, i.e. the relative area of features within the cell is not taken into account. Connectivity was defined as road area per cell. Furthermore, an approximate number of intersections was computed. Intersections were identified as the centroids of areas with at least five road pixels in a 3x3 pixels window based on the skeleton (only centerlines) of a raster containing the road class. Centerlines were computed using the 'skeletonize' tool from the 'skimage' package in Python. The number of intersections per cell is a second measure of connectivity.

2.2.7 Predictive Modelling and Urban Textures Classification

To investigate the relationship between urban parameters and urban texture, a random forest model was created based on urban parameters derived from remote sensing data and a reference dataset (s. Chapter 2.1, Figure 2). The urban parameters derived from literature (s. Chapter 1.2) as well as the NDVI and MBI were rasterized, resampled to a pixel size of 10x10 m, and stacked. Then, a random forest model was trained to predict urban texture using a random sample of 5 % of the pixels and the provided manually classified texture (s. Figure 2). Accuracy was computed based on the 95 % pixels not used for training. Beside the overall accuracy and Cohen's Kappa coefficient, per-class user's and producer's accuracies were calculated. The producer's accuracy describes how many of the reference pixels were correctly classified and the user's accuracy how many of the pixels classified as a certain class actually belong to that class.
The importance of different parameters was assessed by the mean decrease of accuracy and the mean decrease of Gini. Gini describes the usefulness of a variable by testing if it is able to split mixed labeled nodes into pure single-class nodes; it is a measure of purity after each split. Gini is calculated separately for each input parameter in R; it does not indicate redundancy of correlated variables. The model was then applied to the entire dataset as well as the texture metrics calculated for the second area of interest, Quito, for which no reference classification of types of urban form is available. Furthermore, zonal statistics for each type of texture were computed with the reference texture and urban parameters of Cuenca.

3 Results

3.1 Land Cover Classification

In this section, the results of the four image classification techniques are presented in detail.

3.1.1 Random Forest

Random forest classification produced an overall accuracy of 0.74 with three classes (buildings, roads, background) with a Cohen's Kappa coefficient of 0.46 with Sentinel 2 imagery and an overall accuracy of 0.80 with a Kappa coefficient of 0.60 with PlanetScope 2 imagery. The result very slightly improved when adding the MBI and NDVI to the input dataset. For Sentinel 2, the indices could not improve the result. Shadows were often misclassified as water. This is especially noticeable in the historic centre of Cuenca where streets between dense buildings are in shadow. Overall, urban areas were rather underestimated (s. Table 3, Appendix B).

Table 3: Confusion matrix random forest classification with PlanetScope 2 and Sentinel 2 with NDVI and MBI, Cuenca. Rows: Predicted, columns: Ground truth.

	PlanetScope 2			Sentinel 2		
	Building	Road	Background	Building	Road	Background
Building	34	0	1	32	2	2
Road	9	18	3	14	3	2
Background	17	18	146	14	31	146

3.1.2 Spectral Mixture Analysis

'Pure' pixels are mainly located in the corners of a scatterplot of the first two principal components (Figure 4). However, urban classes are relatively close together. Especially red bricks, bare soil, and asphalt appear to be similar. Thus, some confusion between these classes was to be expected. A comparison between urban classes as derived from the data and spectral profiles derived from the USGS Spectral Library shows similarities, especially between Sentinel 2 and the spectral library (U.S. Department of the Interior - U.S. Geological Survey, 2017) (s. Appendix A). The large differences in bands 9 and 10 are due to these bands being used for water vapor and cloud detection; they do not contain surface information. For PlanetScope 2, reflectance was lower overall since no atmospheric correction was applied to these images (s. Appendix A).

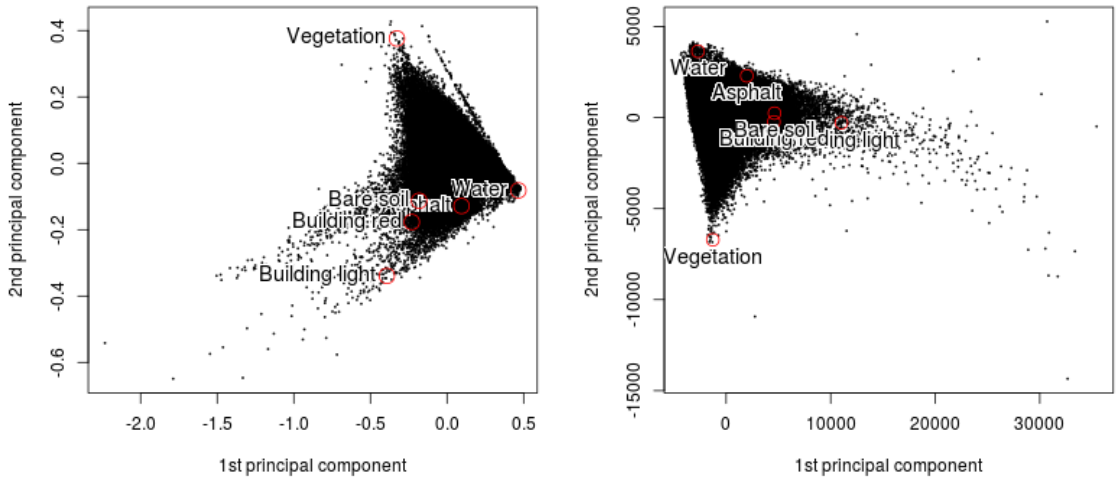

(a) Sentinel 2

(b) PlanetScope 2

Figure 4: 'Pure' pixels' location in the feature space of the first two principal components, Cuenca.

With Sentinel 2 imagery, a distinction between buildings, asphalt, and background yielded an overall accuracy of 0.52 which corresponds to a Kappa of 0.24, the main source of error being misclassification of background classes as asphalt. This is most likely due to the similarity of the spectral profiles of asphalt and bare soil (s. Figure 4 (a)). The classification result based on SMA of PlanetScope 2 imagery had an overall accuracy of 0.56 with a Cohen's Kappa coefficient of 0.44 with all six classes (red building, gray building, asphalt, vegetation, bare soil, and water). The distinction between buildings, asphalt, and background had an overall accuracy of 0.69 and a Cohen's Kappa coefficient of 0.50. The main source of error appears to be an over-estimation of the occurrence of the asphalt class (s. Table 4). Furthermore, the validation dataset was classified by land cover classes rather than surface materials. It was assumed that the road class is equivalent to the surface material asphalt. However, some dirt roads exist in the area of interest so that validation of roads with SMA is conservative. The occurrence of the building classes was strongly underestimated (s. Table 4).

3.1.3 Object-Based Image Analysis

Different segmentation algorithms produced very different results (s. Figure 5). Some results were not valid, i.e. only one or two segments were produced, or there were memory errors even after adapting all possible parameters. Other results were valid, but did not meet the requirement that at least large and characteristic structures should be visu-

Table 4: Confusion matrix SMA with PlanetScope 2 and Sentinel 2, Cuenca. Rows: Predicted, columns: Ground truth.

	PlanetScope 2			Sentinel 2		
	Building	Road	Background	Building	Road	Background
Building	43	12	17	17	0	2
Road	17	23	30	30	24	62
Background	0	1	103	13	12	86

ally recognizable (s. Table 5). Out of the valid and visually interpretable results, some lacked detail or showed signs of oversegmentation. The watershed algorithm in combination with PlanetScope 2 (dataset no°4 in Chapter 2.2.4.3) and PlanetScope 2 with Sentinel 2 (dataset no°5 in Chapter 2.2.4.3) datasets produced segmentation results which allowed to distinguish between dense urban areas and more homogenous rural parts of the study area. Edge enhancement and the addition of the MBI and NDVI improved the result. Segmentation of an image composed only of MBI and NDVI looked similar to segmentation including spectral bands in urban areas. Segmentation results of Sentinel 2 data alone lacked detail and were therefore discarded.

Table 5: Results of image segmentation with different datasets and segmentation algorithms, Cuenca. +: Certain characteristic features (e.g. the airport landing strip) can be recognized visually with basic knowledge of the area of interest; o: Valid result, but not visually interpretable; -: Invalid.

	Hierarchical Region Growing (GRASS)	Meanshift (OTB)	Morphological-Based (OTB)	Shepherd / k-means (RSGISLib)	Watershed (OTB)
1. Sentinel 2	o	-	o	o	o
2. Sentinel 2 + Sentinel 1	o	o	o	o	o
3. Band reduced Sentinel 1 + 2	o	o	+	+	-
4. PlanetScope 2	+	o	-	+	+
5. PlanetScope 2 + Sentinel 2	+	-	o	o	+
6. PlanetScope 2 + Sentinel 1 + 2	o	-	o	o	-
7. Sentinel 2, edge enhanced, NDVI	o	-	o	o	o
8. PlanetScope 2, edge enhanced, NDVI	+	o	o	+	+

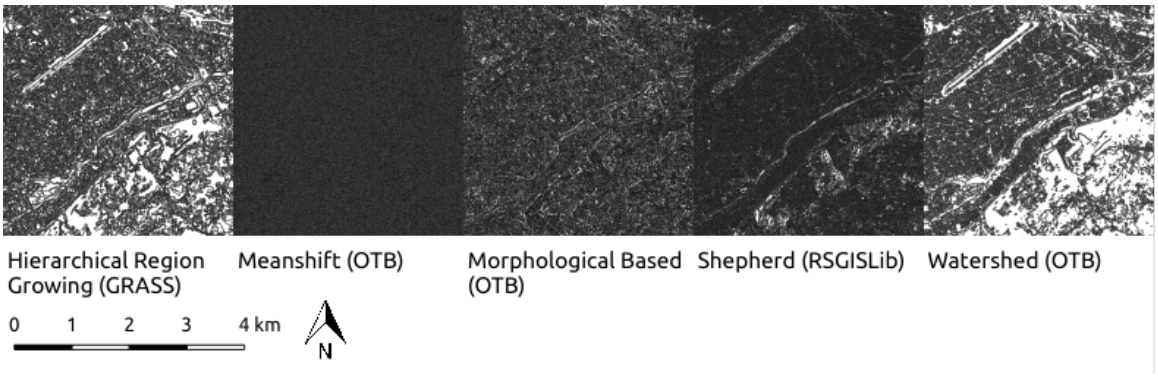

Figure 5: Different segmentation results based on PlanetScope 2 imagery of Cuenca with a Touzi edge enhancement band. The maps show the south east of Cuenca, the linear structure in the north-western corner being the airport.

The best result of feature classification using an ANN was achieved based on PlanetScope 2 spectral bands with an NDVI and a Touzi filtered band segmented with the watershed algorithm. The classification had an overall accuracy of 0.56 with a Kappa of 0.46 with six classes (building - red brick roof, building - light / gray, road, bare soil, vegetation, forest, water; s. Appendix C). When summarizing the result to the two classes of interest - buildings and roads - and a background class, the overall accuracy increased to 0.79 and the Kappa to 0.60 (s. also table 6). Combined PlanetScope 2 and Sentinel 2 data produced an overall accuracy of 0.55 and a Cohen's Kappa coefficient of 0.45 and thus qualified as the second best result. The improvement compared to PlanetScope 2 without Sentinel 2 is marginal (Kappa: 0.44). Overall, the technique performed slightly less well than random forest classification but better than SMA. Sentinel 1 texture metrics did not improve the result which might be due to the lower spatial resolution of these data (s. Chapter 2.1). A disadvantage of watershed segmentation is a tendency to oversegment linear features so that shape metrics cannot be taken into account for classification.

Table 6: Confusion matrix OBIA with PlanetScope 2 with NDVI and Touzi filtered bands, Cuenca. Rows: Predicted, columns: Ground truth.

	Building	Road	Background
Building	34	1	0
Road	16	19	9
Background	10	16	141

3.1.4 Thresholding and ANN

Thresholding combined with ANN classification based on indices and shape metrics produced an overall accuracy of 0.77 and a Cohen's Kappa coefficient of 0.57 with Sentinel 2 images and three classes (building, road, and background). With PlanetScope 2 data, an overall accuracy of 0.80 with a Kappa coefficient of 0.66 with four classes (building, road, vegetation, and water) was achieved (s. Table 7, figure 6). When summarizing vegetation and water to one background class for more comparability with random forest, the accuracy is 0.81 with a Kappa of 0.67. Thus, the technique produces the best classification results in terms of accuracy. Therefore, the same technique with the same thresholds was applied to Planet imagery of Quito (s. Figure 7). Due to the different landscape surrounding Quito, the water class was replaced by a bare soil class. The result has an overall accuracy of 0.68 with a Cohen's Kappa of 0.56. Summarizing vegetation and bare soil to one background improved the overall accuracy to 0.74 with the same Kappa coefficient. Many classification errors are due to an overestimation of the road class. About 29% of validation points of class building and 47% of class bare soil were misclassified as road (s. Table 8). Unlike in Cuenca, most buildings in Quito have a gray roof so that the RI is not sufficient to distinguish between buildings and roads. Furthermore, bare soil occurs more often than in Cuenca so that the NDVI alone is not sufficient to distinguish between background classes and roads. The MBI only excludes large areas of bare soil. The thresholds used for the initial classification were:

- Initial building or light road: MBI >= 600 and NDVI < 0.1
- Initial red brick building: MBI >= 600 and NDVI < 0.1 and RI >= 0 (this is a subset of initial building / light road)
- Initial shadowy road: Black Top Hat >= 1000 and NDVI < 0.1
- Initial vegetation: NDVI >= 0.1

with PlanetScope 2 and:

- Initial building or light road: MBI >= 10 and NDVI < 0.3
- Initial red brick building: MBI >= 10 and NDVI < 0.3 and RI > 0.1 (this is a subset of initial building / light road)
- Initial shadowy road: Black Top Hat >= 100 and NDVI < 0.3
- Initial vegetation: NDVI >= 0.3

with Sentinel 2 data.

Table 7: Confusion matrix Thresholding and ANN with PlanetScope 2 and Sentinel 2, Cuenca. Rows: Predicted, columns: Ground truth.

	PlanetScope 2			Sentinel 2		
	Building	Road	Background	Building	Road	Background
Building	46	7	19	41	15	13
Road	11	26	4	10	13	2
Background	3	3	127	9	8	135

Table 8: Confusion matrix of classification based on PlanetScope 2 images with indices and shape metrics, Quito. Rows: Predicted, columns: Ground truth.

	Building	Road	Vegetation	Bare Soil
Building	30	3	1	1
Road	18	34	0	14
Vegetation	3	5	87	15
Bare Soil	12	7	0	16

3.1.5 Comparison

Large differences between the four land cover classification methods were observed. The highest accuracy was achieved using a classification method based on thresholding with indices followed by feature classification with an artificial neural network (s. Chapters 2.2.4.4 and 3.1.4, figures 6 and 7, table 9).

Table 9: Highest accuracies achieved with different land cover classification techniques, Cuenca.

Classification technique	PlanetScope 2		Sentinel 2	
	Overall accuracy	Cohen's Kappa	Overall accuracy	Cohen's Kappa
SMA	0.69	0.50	0.52	0.24
Random forest	0.80	0.60	0.74	0.46
OBIA	0.79	0.60	N.A.	N.A.
Indices & shape metrics	0.81	0.67	0.77	0.57

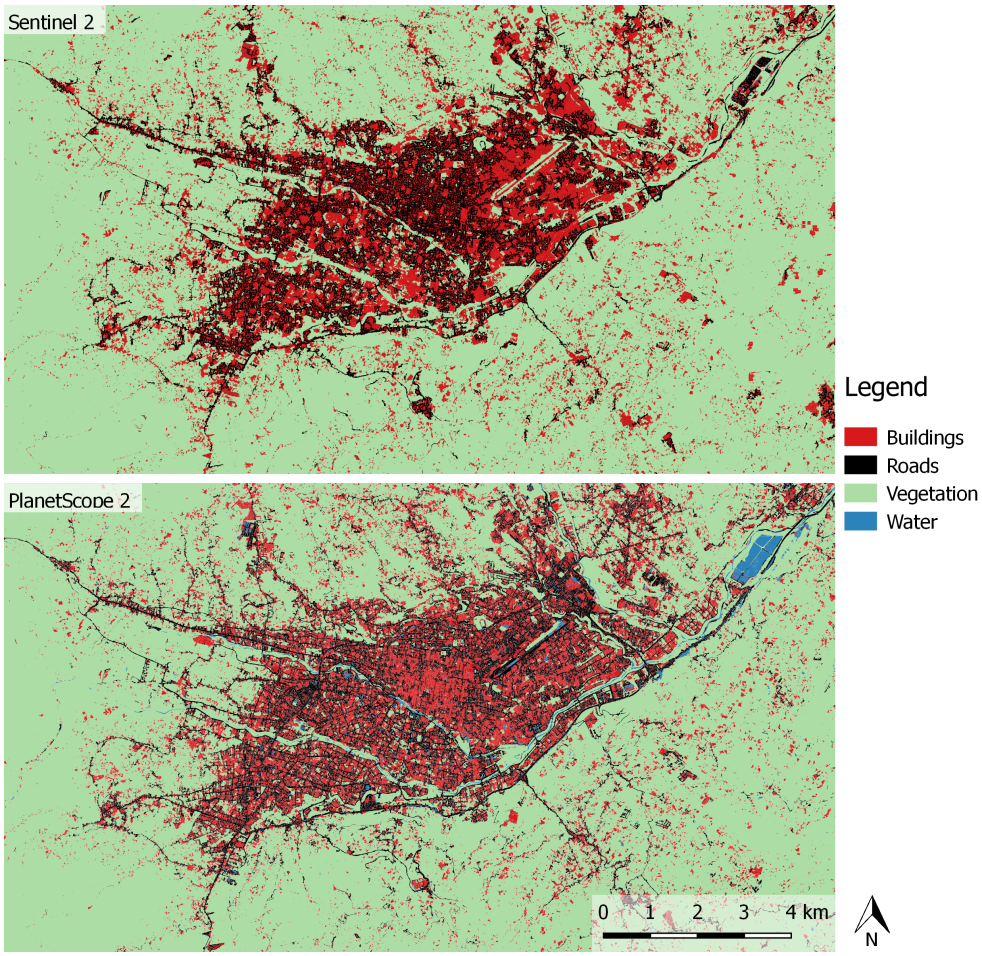

Figure 6: Classification results based on indices and shape metrics classified with thresholds and ANN, Cuenca.

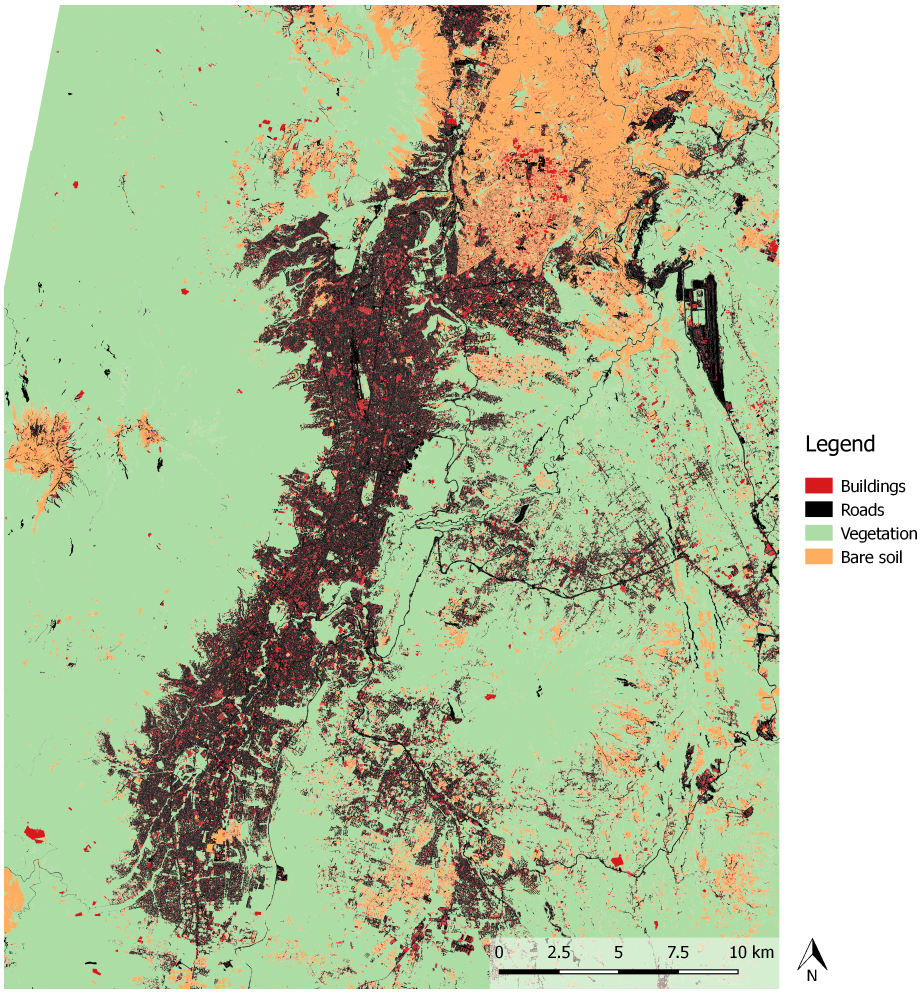

Figure 7: Classification result based on indices and shape metrics classified with thresholds and ANN, based on PlanetScope 2 images, Quito.

3.2 Urban Parameters

The best classification result chosen for parameter extraction is adaptive thresholding and ANN classification with shape metrics and MBI (s. Chapter 3.1.4, Figures 6 and 7). Density (feature count), density (percentage of urban area), connectivity (road area), connectivity (number of intersections), and compactness were computed based on this result. Furthermore, the MBI and NDVI were derived from PlanetScope 2 imagery. Roughness was calculated based on the DEM using equation 6. All eight parameters show a clear distinction between urban and non-urban areas. Compactness, connectvity and density, in particular, also show differences between different parts of the city. Differences between the classification results of both study areas are visible as well (s. Figures 8 and 9). In Quito, road area was overestimated (s. Table 8). As a result, connectivity is less differentiated than in Cuenca. The distinction of urban area by NDVI is also more difficult in Quito due to the presence of bare mountainous areas and volcanoes in its surroundings. Overall, the lower classification accuracy is reflected in the urban parameters (s. Figure 9).

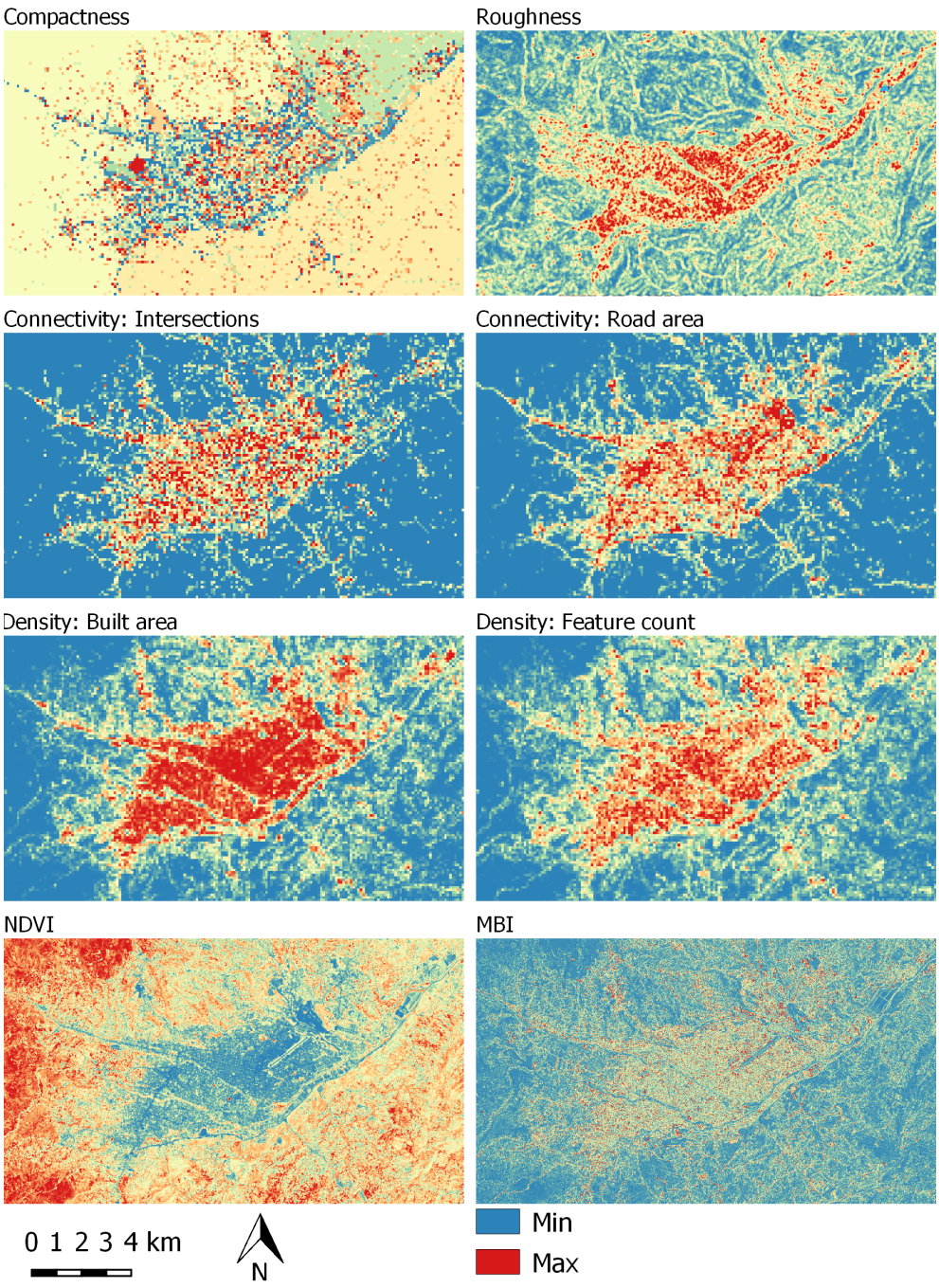

Figure 8: Urban parameters related to texture, Cuenca.

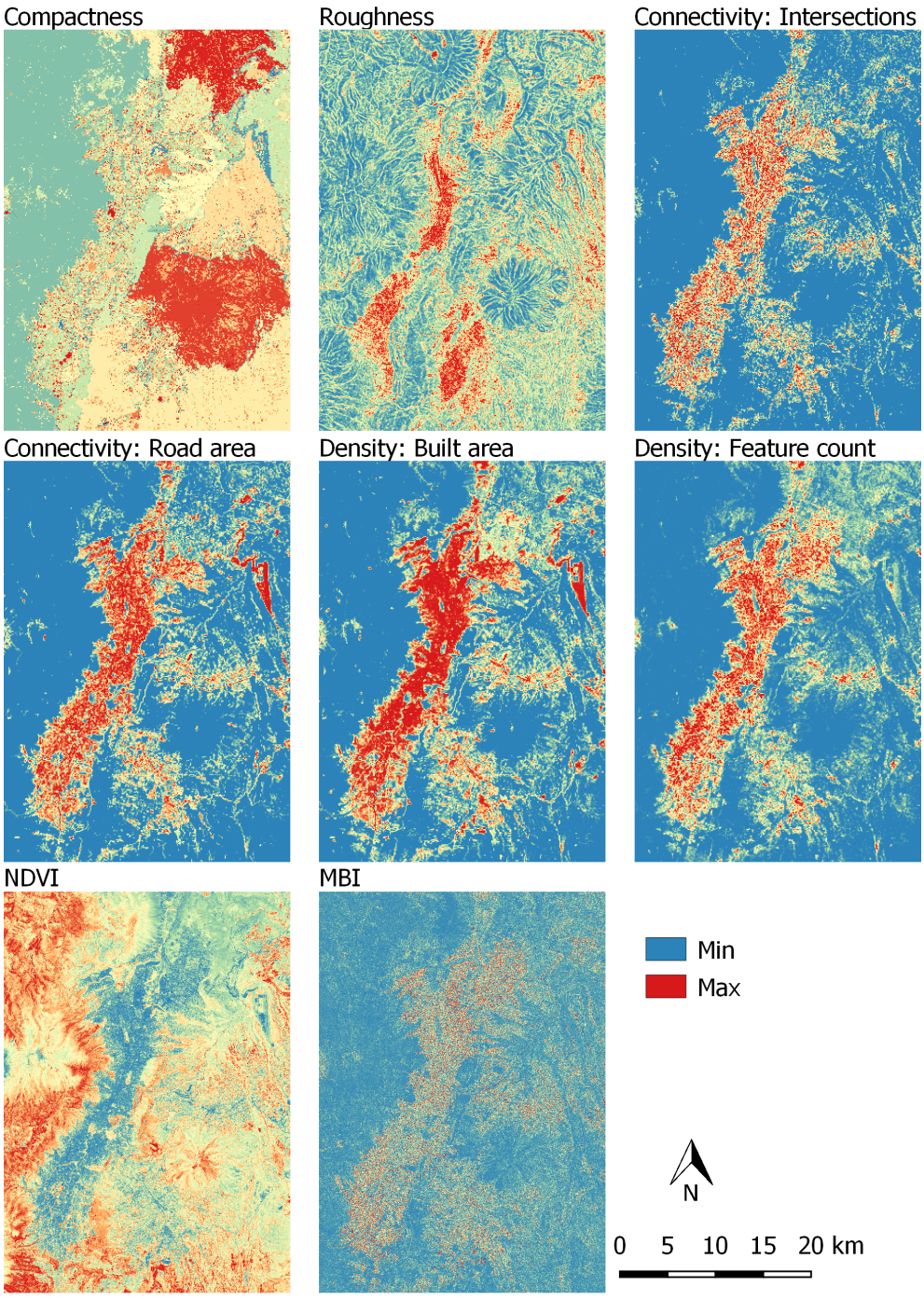

Figure 9: Urban parameters related to texture, Quito.

3.3 Detecting Urban Textures

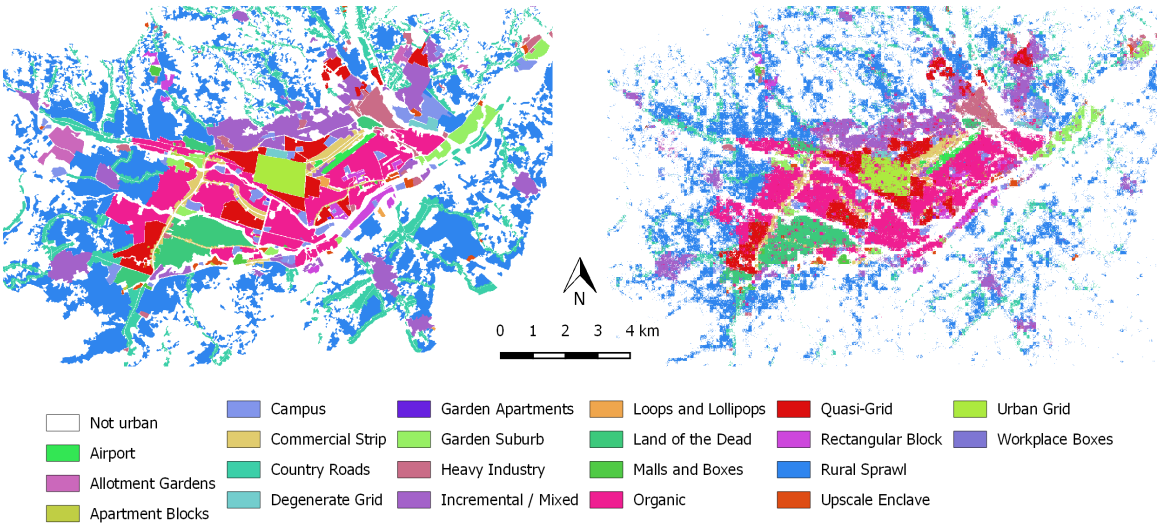

Figure 10: Left: Manual classification of urban textures used as reference. Right: Urban textures detected using Random Forest Classification with the eight urban parameters as inputs. Cuenca.

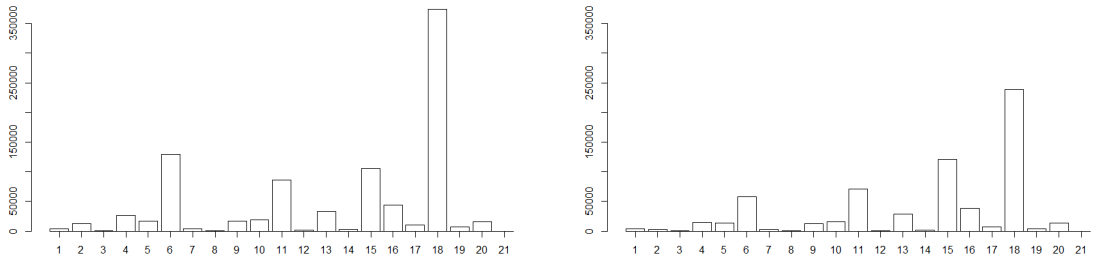

(a) Reference (b) Predicted

Figure 11: Frequency of texture classes in Cuenca. 1: Airport, 2: Allotment Gardens, 3: Apartment Blocks, 4: Campus, 5: Commercial Strip, 6: Country Roads, 7: Degenerate Grid, 8: Garden Apartments, 9: Garden Suburb, 10: Heavy Industry, 11: Incremental / Mixed, 12: Loops and Lollipops, 13: Land of the Dead, 14: Malls and Boxes, 15: Organic, 16: Quasi-Grid, 17: Rectangular Block, 18: Rural Sprawl, 19: Upscale Enclave, 20: Urban Grid, 21: Workplace Boxes.

Texture could be predicted with an overall accuracy of 0.79 and a Cohen's Kappa co-

efficient of 0.61 (s. Figure 10) in Cuenca with a random forest model trained on 5 % of pixels from the parameter stack and reference texture. Urban area was underestimated, especially the classes 'Country Roads' and 'Rural Sprawl' which have the largest spatial coverage in the reference image. The class 'Organic' was overestimated (s. Figures 10 and 11, table 10). Density (feature count), density (urban area per cell), and connectivity (road area) had the greatest influence on classification accuracy whereas roughness, the MBI and the NDVI had the least influence (s. Table 11). The NDVI had a relatively high mean decrease of Gini value but a low mean decrease of accuracy value (ibid). This may indicate redundancy of the variable; according to Figure 12, it might be highly correlated with density. In spite of its low values, leaving out roughness reduced the accuracy to 0.58 and Cohen's Kappa coefficient to 0.23. Therefore, all parameters appear to be correlated with urban texture to some extent.

Table 10: Confusion matrix and per-class accuracies of urban texture prediction, Cuenca. Rows: Predicted, columns: Reference. Classes: 0: Not urban, 1: Airport, 2: Allotment Gardens, 3: Apartment Blocks, 4: Campus, 5: Commercial Strip, 6: Country Roads, 7: Degenerate Grid, 8: Garden Apartments, 9: Garden Suburb, 10: Heavy Industry, 11: Incremental / Mixed, 12: Loops and Lollipops, 13: Land of the Dead, 14: Malls and Boxes, 15: Organic, 16: Quasi-Grid, 17: Rectangular Block, 18: Rural Sprawl, 19: Upscale Enclave, 20: Urban Grid, 21: Workplace Boxes.

	0	1	2	3	4	5	6	7	8	9	10	11	12	13	14	15	16	17	18	19	20	21
0	1261-133	618	8179	155	9056	2789	67038	432	140	3471	3,576	17038	436	1948	380	9515	2612	1505	191-096	2337	119	3
1	191	2618	0	0	7	25	1	0	0	0	12	36	3	0	0	252	0	0	0	0	0	0
2	152	0	1800	0	0	0	3	0	0	0	0	44	0	0	0	0	13	0	2	0	0	0
3	63	0	0	301	0	0	0	0	0	20	0	0	0	18	0	12	32	9	6	32	0	0
4	1002	11	0	0	11829	62	77	45	3	39	15	176	0	12	0	295	56	27	115	25	31	0
5	2404	129	3	2	130	8738	18	1	0	44	94	193	1	290	16	711	315	71	26	4	15	0
6	9209	1	63	6	99	15	37784	3	1	138	127	630	0	35	3	317	236	15	2910	116	0	0
7	179	0	1	0	18	0	0	2111	0	0	0	9	0	1	0	2	0	3	0	0	78	0
8	27	0	0	0	4	0	0	0	57	0	0	0	0	0	0	0	25	0	0	0	0	0
9	864	0	4	0	60	12	9	0	0	10375	26	12	0	0	2	80	7	0	13	30	0	0
10	1034	44	2	3	81	357	77	13	0	24	12801	197	0	38	234	160	78	8	79	40	8	0
11	4628	45	60	2	530	294	914	255	10	217	383	53859	40	668	5	1685	1353	258	1470	165	38	0
12	34	0	0	0	0	0	0	0	0	0	0	0	490	0	0	7	1	0	0	0	0	0
13	997	0	4	0	51	675	29	0	0	59	60	102	0	24637	11	405	316	12	53	4	4	0
14	175	0	0	0	0	16	51	0	0	0	2	0	0	39	1657	8	0	4	40	1	0	0
15	8467	132	58	127	1487	2885	753	495	48	1467	658	2699	80	2850	179	84346	4205	1421	970	223	1843	32
16	2233	0	8	32	197	428	94	46	14	13	59	664	23	266	10	742	31145	213	33	97	411	2
17	521	0	1	4	25	21	10	0	0	3	0	2	0	0	9	43	86	5744	38	0	1	0
18	33607	4	1251	11	1320	91	16455	63	6	476	344	5720	173	671	52	2075	326	467	157-770	647	0	0
19	319	0	0	7	20	1	48	0	0	5	36	0	0	3	0	1	1	0	57	3013	0	0
20	266	0	0	1	37	46	0	68	0	6	57	31	0	22	0	189	339	71	6	1	12067	0
21	2	0	0	0	0	0	0	0	0	0	0	0	0	0	0	2	0	0	0	0	0	4
User's acc.	0.80	0.83	0.89	0.61	0.86	0.66	0.73	0.88	0.50	0.90	0.84	0.81	0.92	0.90	0.83	0.73	0.85	0.88	0.71	0.86	0.91	0.50
Producer's acc.	0.95	0.73	0.16	0.46	0.47	0.53	0.31	0.60	0.20	0.63	0.70	0.66	0.39	0.78	0.65	0.84	0.76	0.58	0.44	0.45	0.83	0.10

Table 11: Importance of different input parameters.

Parameter	Mean Decrease of Accuracy	Mean Decrease Gini
Compactness	0.06576611	6071.266
Roughness	0.05228191	7992.453
Connectivity; number of intersections	0.05997891	3772.212
Connectivity; road area	0.09905073	8127.111
Density; area	0.11658440	12171.032
Density; count	0.14058516	10468.657
NDVI	0.04013470	8164.336
MBI	0.02374680	7398.652

To further explore the correlation, zonal statistics per texture class and urban parameter were computed. None of the individual parameters allows separability between classes, but differences are visible (s. Figure 12). For instance, areas classified as 'Rural Sprawl' have a high average NDVI and a low density and connectivity whereas 'Urban Grid' is especially compact and contains a high number of urban features.

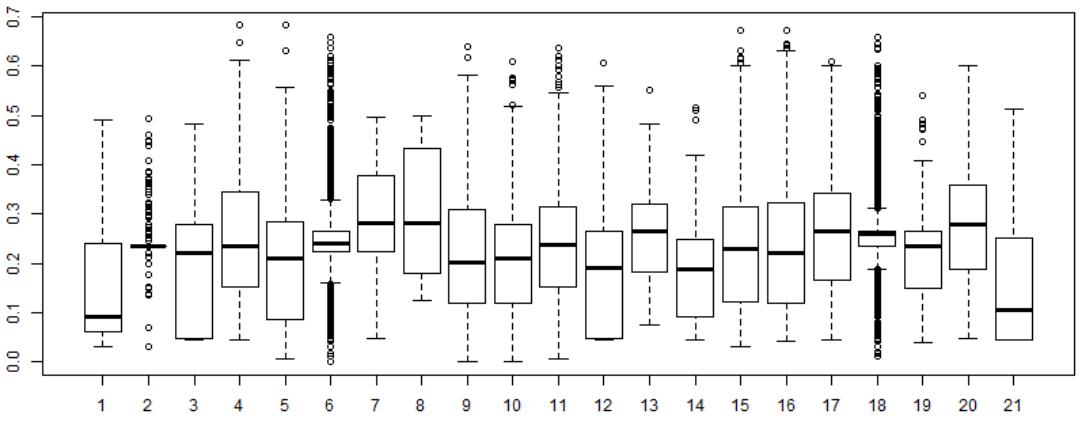

(a) Compactness by class.

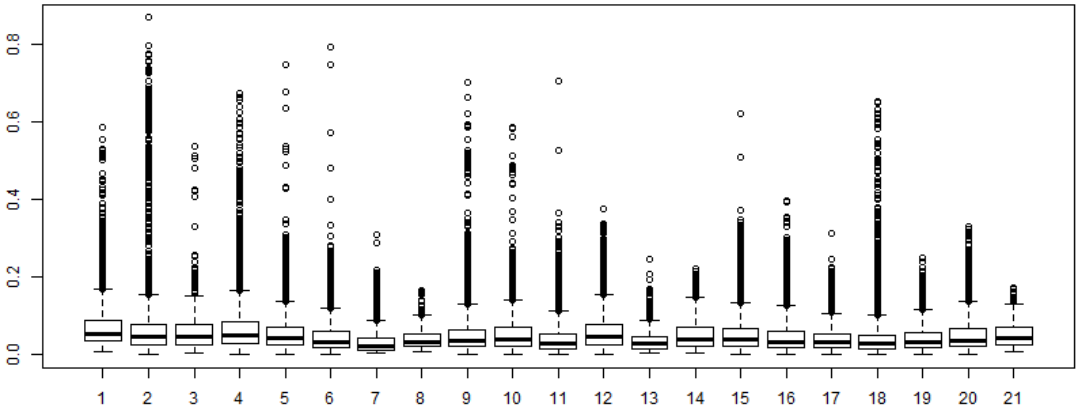

(b) Roughness by class.

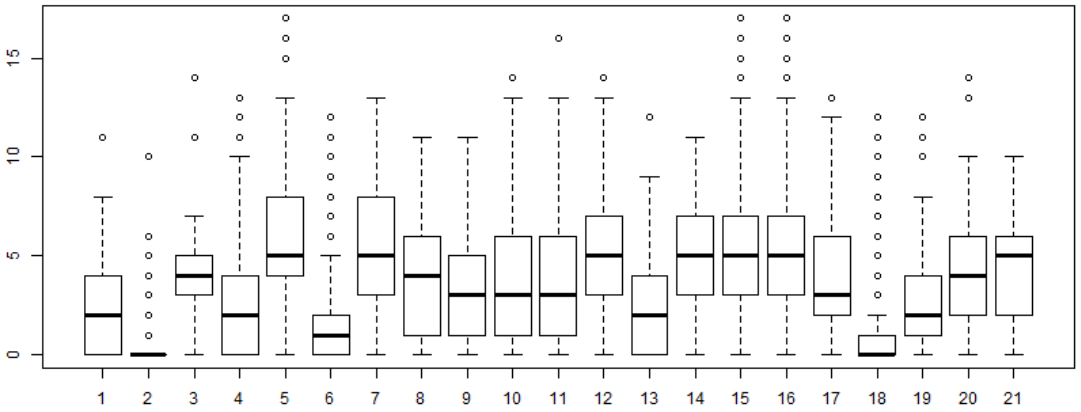

(c) Number of intersections by class.

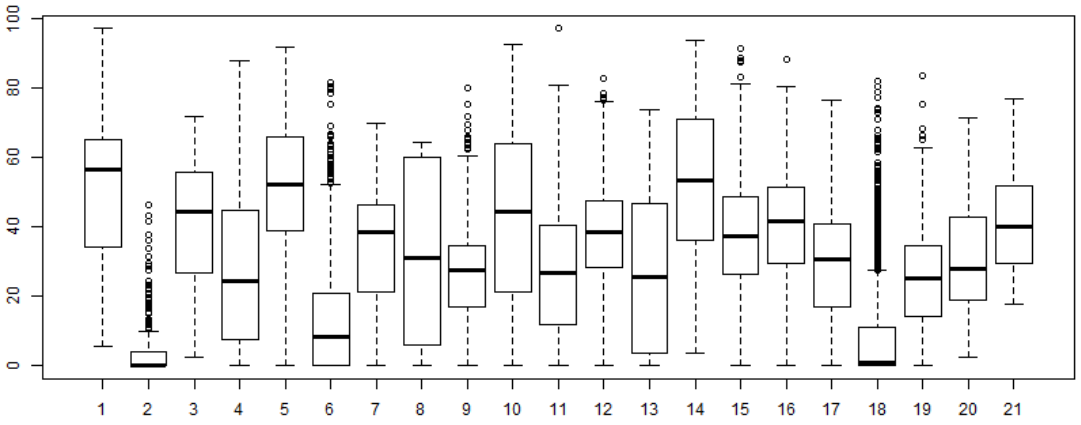

(d) Road area by class.

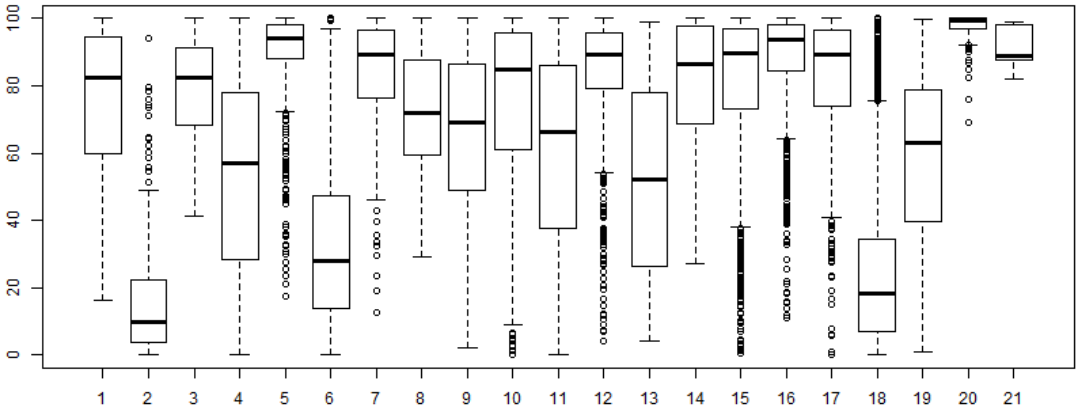

(e) Density as percentage of built area per cell by class.

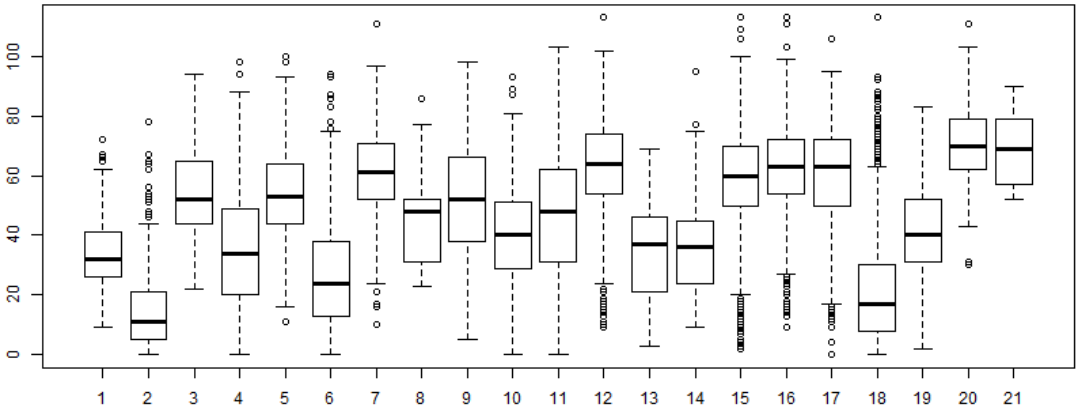

(f) Density as number of urban features per cell by class.

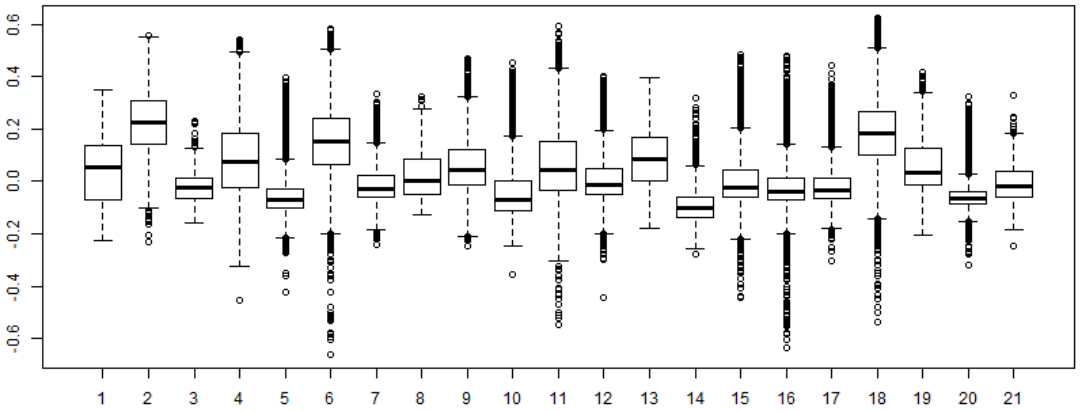

(g) NDVI by class.

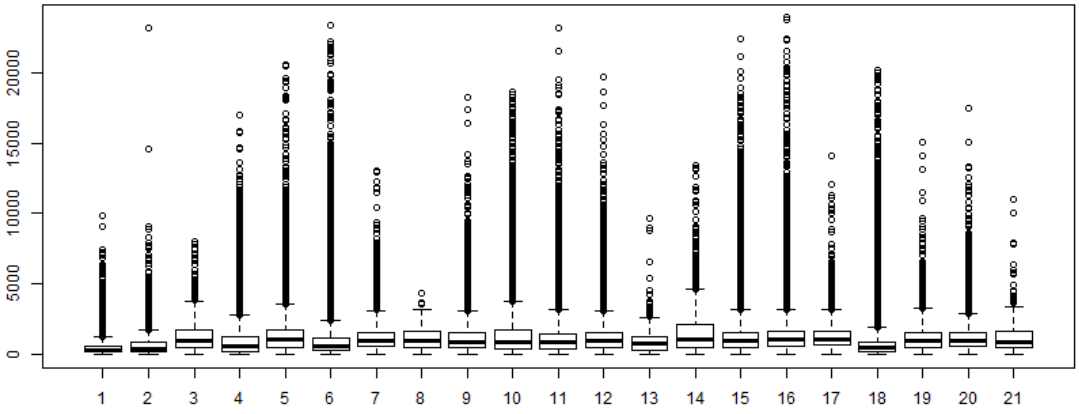

(h) MBI by class.

Figure 12: Value distribution of urban parameters by reference texture class, Cuenca. 1: Airport, 2: Allotment Gardens, 3: Apartment Blocks, 4: Campus, 5: Commercial Strip, 6: Country Roads, 7: Degenerate Grid, 8: Garden Apartments, 9: Garden Suburb, 10: Heavy Industry, 11: Incremental / Mixed, 12: Loops and Lollipops, 13: Land of the Dead, 14: Malls and Boxes, 15: Organic, 16: Quasi-Grid, 17: Rectangular Block, 18: Rural Sprawl, 19: Upscale Enclave, 20: Urban Grid, 21: Workplace Boxes.

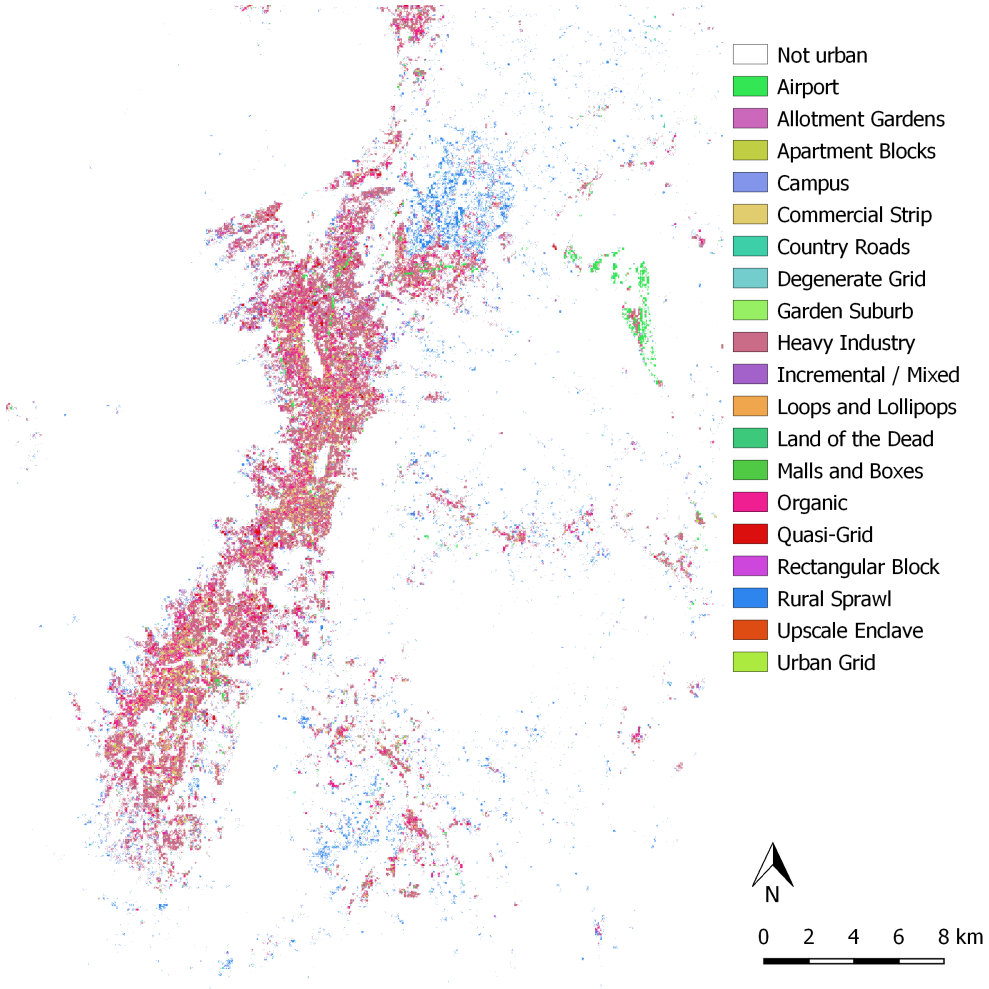

Figure 13: Predicted urban texture classes, Quito.

Since no reference urban texture classification data was available for Quito, the model trained with data from Cuenca was applied to detect urban textures in this city (s. Figure 13). The class with the greatest coverage is 'Heavy Industry'. Large streets within the city were classified as 'Airport'. Another class with large coverage is 'Organic'. 'Rural Sprawl' and 'Upscale Enclaves' appear near the edges of the city. 'Garden Apartments' and 'Workplace Boxes' are not present in the prediction in spite of being present in the manual classification of Cuenca (s. Figure 14). The airport of Quito and rural sprawl were partly correctly classified.

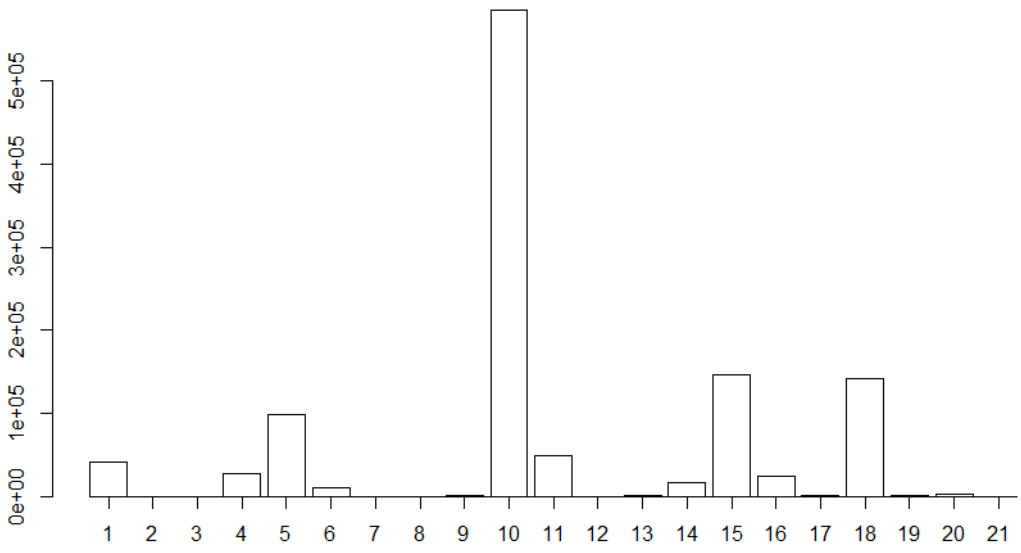

Figure 14: Texture in Quito. 1: Airport, 2: Allotment Gardens, 3: Apartment Blocks, 4: Campus, 5: Commercial Strip, 6: Country Roads, 7: Degenerate Grid, 8: Garden Apartments (count equals zero), 9: Garden Suburb, 10: Heavy Industry, 11: Incremental / Mixed, 12: Loops and Lollipops, 13: Land of the Dead, 14: Malls and Boxes, 15: Organic, 16: Quasi-Grid, 17: Rectangular Block, 18: Rural Sprawl, 19: Upscale Enclave, 20: Urban Grid, 21: Workplace Boxes (count equals zero).

4 Discussion

4.1 Land Cover Classification

In Latin America, a trend of urban expansion combined with a decrease of density in cities has been observed (Inostroza et al., 2013). This coincides with the analysis of urban form in Cuenca and Quito which showed that urban sprawl towards rural areas (i.e. the texture class 'Rural Sprawl') plays an important role in these cities. This development poses new challenges for urban planning, specifically with regard to transportation choices. Therefore, it is important to get a better understanding of urban areas. Extraction of impervious surfaces has been widely used for the analysis of urban development. Object-based classification was shown to be suitable for this task (Benítez et al., 2018; Sugg et al., 2014). However, a more detailed classification is necessary for urban texture analysis. Different classification techniques were compared in this research. It was found that object-based approaches based on open mid-resolution and commercial high-resolution remote sensing data are too coarse to extract features like individual buildings and roads. This confirms former findings which imply that OBIA is successful when objects of interest are considerably larger than the pixel size (Blaschke, 2010). Benítez et al. (2018) found that OBIA performed better than sub-pixel classification of impervious surfaces based on mid-resolution remote sensing data. This was confirmed by our research (s. Appendix A, Appendix C). Pixel based classification with random forest performed better than both sub-pixel and object-based approaches (s. Chapter 3.1.2). The suggested method combining pixel-based classification based on both spectral and morphological properties with object-based classification based on shape metrics produced the best results for Cuenca (s. Chapter 3.1.4). However, the approach is significanty less successful when applied to Quito. This might be due to buildings and streets being more difficult to separate in Quito since many buildings have gray roofs. An advantage of the approach is its relatively high accuracy when applied to mid-resolution data. It is the only technique which could produce a Cohen's Kappa coefficient higher than 0.50 with only Sentinel 2 imagery. The low Kappa coefficient of random forest classification in spite of a similar accuracy is due to an overestimation of the background class which has the greatest spatial coverage. This is interpreted as a greater influence of chance by the Kappa calculation. The identification of individual buildings, smaller roads and intersections is only possible with commercial high resolution PlanetScope 2 data. All results lack detail in particularly dense urban areas such as the historic centre of Cuenca.

4.2 Urban Parameters

The urban parameters density, connectivity, and compactness derived from literature (s. Chapter 1.2) can be computed based on a land cover map. Density as urban area per cell has the highest certainty as it is directly derived from the land cover. Density as feature count is less accurate since features of the same class which are next to each other appear

as one feature. Connectivity as road area is similar to density as percentage of built area, but it strongly depends on the separability of urban classes. No validation data for the count of intersections was available, but it can be assumed that accuracy is relatively low since there were several issues during classification. Firstly, the road class was the least accurately classified with an error of omission of 0.28 and an error of commission of 0.37 (s. Table 7). Secondly, skeletonization did not alway extract one exact centerline per road. Especially wide road features with irregular borders led to several centerlines. Finally, narrow curves were sometimes misclassified as intersections. The compactness index describes features well and was useful for feature classification. However, it is strictly on a feature level and cannot be interpreted as compactness of a city as described in chapter 1.2. The addition of NDVI and MBI increased the accuracy of urban texture prediction (s. Table 11), but these parameters can be considered to be strongly correlated to density as percentage of urban area per cell since they were used for land cover classification. Roughness is based on elevation data. Large differences between different parts of the city could be observed (s. Figures 8 and 9). Furthermore, roughness was found to be linked directly to transportation choices in former research (Ng et al., 2011). Unfortunately, available elevation data were considerably older than remote sensing images. This might explain the low importance of roughness for urban texture prediction (s. Table 11).

4.3 Detecting Urban Texture

Urban parameters derived from the classification results were shown to be correlated with urban texture according to a visual classification based on the typology proposed by Wheeler (2015). Density, connectivity and compactness are best suited to predict texture classes (s. Table 11). However, the prediction model was not transferable to the second area of interest, Quito. This might be due to the lower quality of the classification as well as differences between the overall structures of both cities. For instance, very large roads within the city were classified as airport; this is not unreasonable since the airport in Cuenca consists of a single broad landing strip surrounded by buildings. 'Heavy Industry' in Cuenca has a low NDVI, low density in terms of feature count and a low number of intersections, but very high density in terms of urbanized area, especially a high road area (s. Figure 12). This is true for many parts of Quito. 'Rural sprawl' was often correctly classified, but its coverage was underestimated, which was also the case for the prediction of urban texture in Cuenca (s. Figure 11, table 10). The class 'Organic' was overestimated in both cities (s. Figures 11 and 14, table 10) Possibly, a texture prediction model trained on several cities would be applicable to a new area of interest. However, urban parameters extracted in this study cannot describe urban form in its full complexity. They describe urban areas at a pixel and object level whereas urban form is often defined by complex grid and parcel patterns. For instance, road shape, e.g. loops vs. rectangular grid, was not taken into account. Another aspect is the location of a neighborhood within the city, which is only partly expressed by the parameters density and connectivity. Furthermore, socio-economic factors are not always reflected by quantifiable parameters. For instance, a neighborhood with low density, a high NDVI and low connectivity might be a low-income

periferic agricultural neighborhood or an upscale residential area. The difficulty of separating types of urban texture based on urban parameters alone is shown by Figure 12. Variability within a class is usually larger than between-class variability.

5 Conclusion and Recommendations

5.1 Conclusion

In the following paragraphs, the research questions posed at the beginning of this report (s. Chapter 1.3) are discussed in light of our results. All three research questions could be answered satisfactorily.

5.1.1 Which parameters of urban morphology can be extracted from mid-resolution open remote sensing data using open software?

All parameters derived from literature (s. Chapter 1.2), i.e. density, connectivity, roughness, and compactness, could be extracted from remote sensing data. Beside these parameters, the Normalized Difference Vegetation Index (NDVI) and Morphological Building Index (MBI) were investigated. These parameters can easily be computed and add to the accuracy of texture prediction (s. Table 11). Overall shape and size of the city were not quantified, but can be derived from the land cover classification. All parameters were shown to be correlated with urban texture classes according to the typology of Wheeler (2015).

5.1.2 Which analytic methods and techniques are suitable to classify remote sensing images according to these parameters?

Parameter extraction strongly depends on the possibility to accurately classify urban land cover. The best classification result was achieved using initial pixel-based classification based on thresholding of NDVI, MBI, and RI followed by object-based feature classification based on shape metrics with an ANN. The second best result was produced by pixel-based random forest classification.

5.1.3 What is the added value of PlanetScope 2 data as an example of commercial high-resolution remote sensing imagery?

Spatial resolution appears to play a more important role than spectral resolution. Small roads, in particular, could only be extracted from high-resolution commercial imagery. Thus, commercial high resolution imagery significantly improved the quality of urban land cover classification and of urban parameters extracted from it. The added value of PlanetScope 2 compared to Sentinel 2 is an increase in accuracy of 0.04 and a difference between Cohen's Kappa coefficients of 0.10 with indices and shape metrics (s. Chapter 3.1.4). The difference was even more significant with regard to random forest classification (s. Chapter 3.1.1). SMA and OBIA did not produce any usable results with Sentinel 2 data alone.

5.2 Recommendations

Urban parameters that can be extracted from remote sensing data are correlated to types of urban texture. However, this research focused on a limited number of parameters and two study areas with very different structures in spite of both being Andean cities in Ecuador. Thus, results from one city cannot immediately be transferred to another. In future research, different classification approaches such as deep learning should be applied to remote sensing data to improve the accuracy and explanatory power of urban parameters. Furthermore, other parameters such as road shape and angles, number of culs-de-sac, land use and location of neighborhoods within the city could be investigated. To automatically predict urban texture classes according to Wheeler (2015), several study areas need to be used to train a prediction model.

If a larger number of urban texture classifications for training was available, it might be possible to accurately predict types of urban texture, especially if land cover classification accuracy can be increased. However, it is likely that some human intervention will remain necessary since complex shapes need to be analyzed and actual land use as well as socio-economic factors play a role. Another interesting approach could be to investigate the direct link between urban parameters and transportation choices in Andean cities.

Appendices

Appendix A

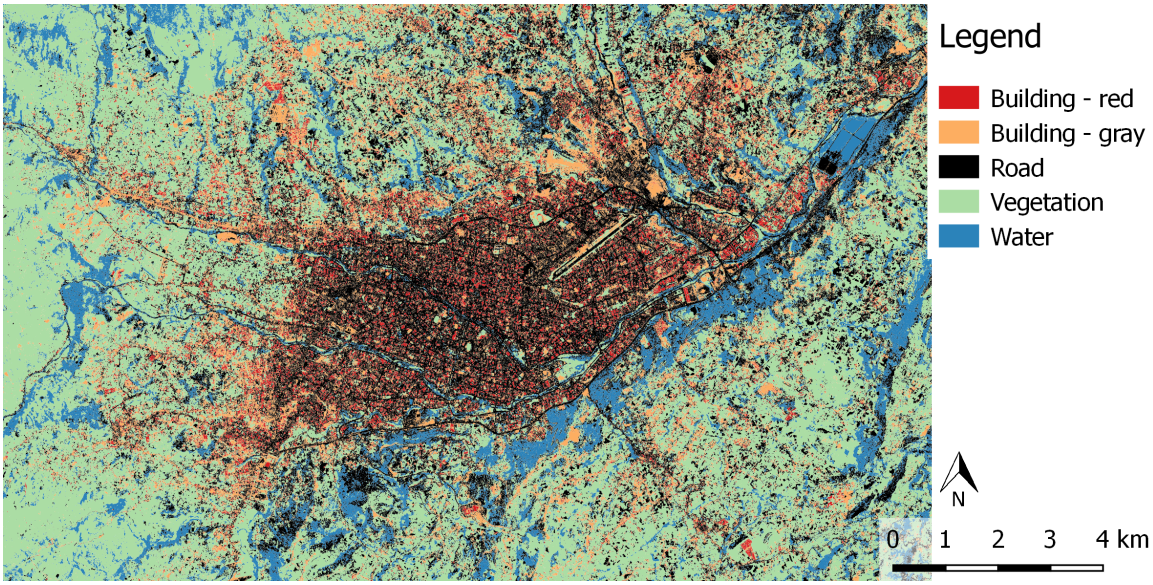

Best classification result, spectral mixture analysis with PlanetScope 2 data, Cuenca.

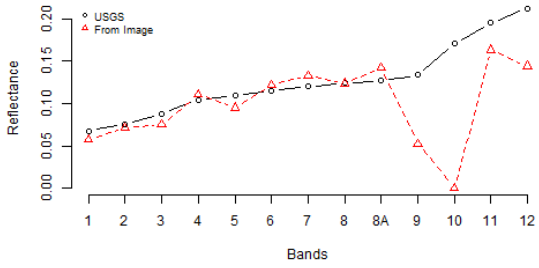

(a) Asphalt: Sentinel 2 vs. USGS

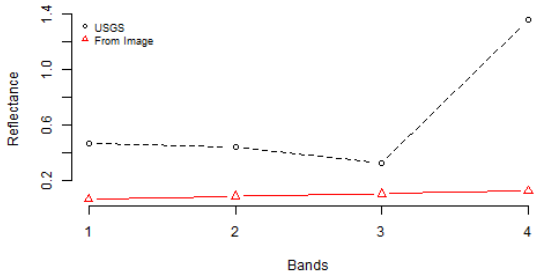

(b) Asphalt: PlanetScope 2 vs. USGS

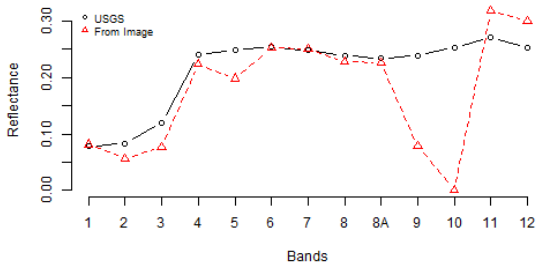

(c) Red bricks: Sentinel 2 vs. USGS

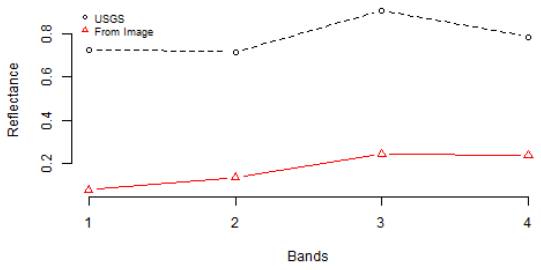

(d) Red bricks: PlanetScope 2 vs. USGS

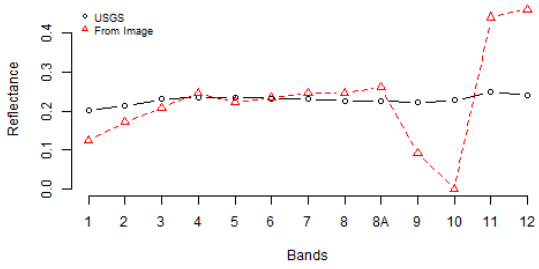

(e) Gray bricks: Sentinel 2 vs. USGS

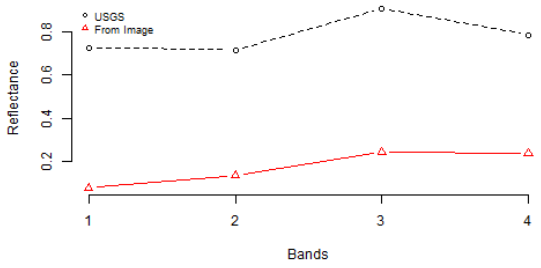

(f) Gray bricks: PlanetScope 2 vs. USGS

Comparison between spectral profiles derived from images and USGS spectral library reference profiles (U.S. Department of the Interior - U.S. Geological Survey, 2017).

Appendix B

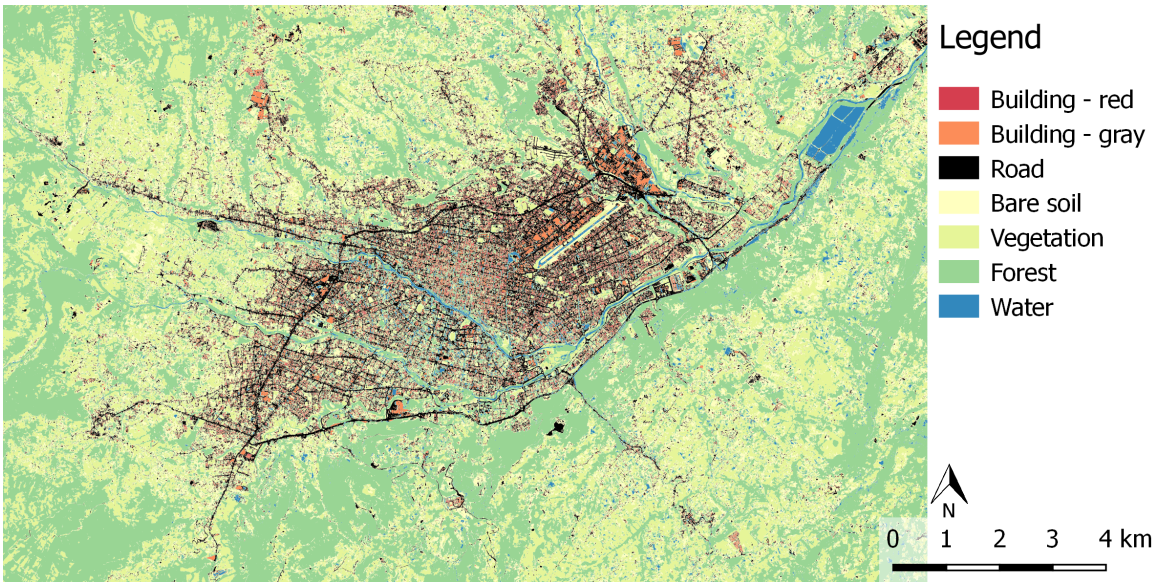

Best classification result, Random forest with PlanetScope 2 including Touzi and NDVI bands, Cuenca.

Appendix C

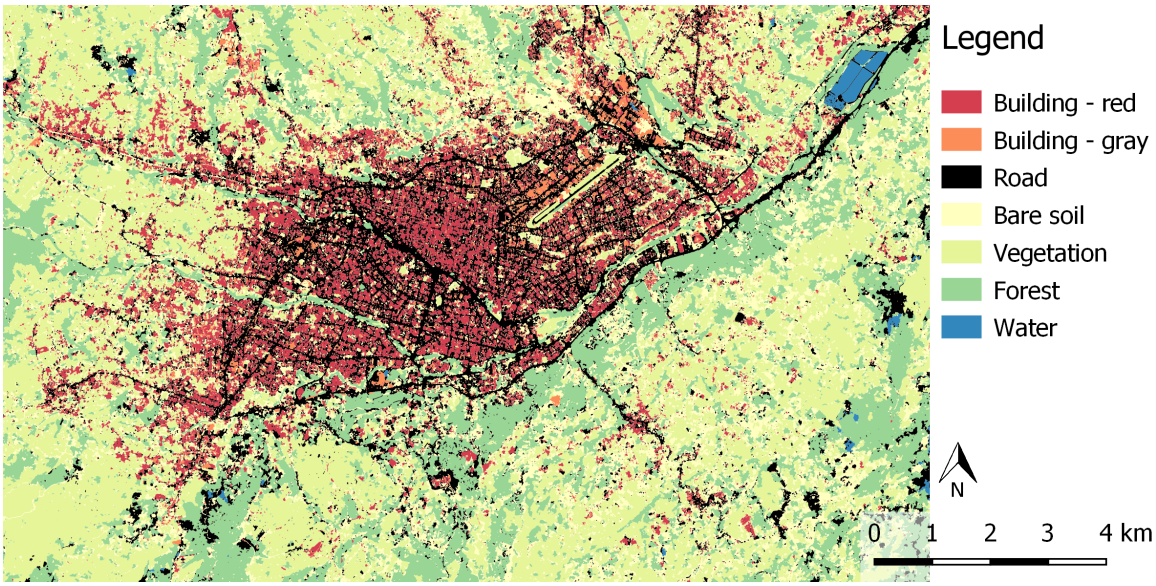

Best classification result, watershed segmentation of combined Sentinel 2 and PlanetScope 2 imagery, classified with ANN, Cuenca.

References

Badland, Hannah M., Schofield, Grant M., and Garrett, Nick (2008). “Travel behavior and objectively measured urban design variables: Associations for adults traveling to work”. In: *Health & Place* 14.1, pp. 85–95. ISSN: 1353-8292. DOI: https://doi.org/10.1016/j.healthplace.2007.05.002. URL: http://www.sciencedirect.com/science/article/pii/S1353829207000354.

Balstad-Miller, Roberta and Small, Christopher (2003). “Cities from space: potential applications of remote sensing in urban environmental research and policy”. In: *Environmental Science & Policy* 6.2, pp. 129–137. ISSN: 1462-9011. DOI: http://dx.doi.org/10.1016/S1462-9011(03)00002-9. URL: http://www.sciencedirect.com/science/article/pii/S1462901103000029.

Benediktsson, Jon Atli, Pesaresi, M., and Amason, K. (2003). “Classification and feature extraction for remote sensing images from urban areas based on morphological transformations”. In: *IEEE Transactions on Geoscience and Remote Sensing* 41.9, pp. 1940–1949. ISSN: 0196-2892. DOI: 10.1109/TGRS.2003.814625.

Benítez, Fátima L., F., Mena Carlos, and Zurita-Arthos, Leo (2018). “Urban Land Cover Change in Ecologically Fragile Environments: The Case of the Galapagos Islands”. In: *Land* 7.21. DOI: 10.3390/land7010021. URL: www.mdpi.com/journal/land.

Bertaud, Alain, Lefèvre, Benoit, and Yuen, Belinda (2009). “GHG Emissions, Urban Mobility and Efficiency of Urban Morphology: A Hypothesis”. In: *Urban Research Symposium 2009 Marseille, France June 28-30, 2009*. URL: AB_BY_BL_Marseille%20Symposium%20Report_5%20.doc.

Bierwagen, Britta G. (2007). “Connectivity in urbanizing landscapes: The importance of habitat configuration, urban area size, and dispersal”. In: *Urban Ecosystems* 10.1, pp. 29–42. ISSN: 1573-1642. DOI: 10.1007/s11252-006-0011-6. URL: https://doi.org/10.1007/s11252-006-0011-6.

Blaschke, T. (2010). “Object based image analysis for remote sensing”. In: *ISPRS Journal of Photogrammetry and Remote Sensing* 65.1, pp. 2–16. ISSN: 0924-2716. DOI: https://doi.org/10.1016/j.isprsjprs.2009.06.004. URL: http://www.sciencedirect.com/science/article/pii/S0924271609000884.

Brachtl, Megan V., Durant, John L., Paez-Perez, Carlos, Oviedo, Jorge, Sempertegui, Fernando, Naumova, Elena N., and Griffiths, Jeffrey K. (2009). “Spatial and temporal variations and mobile source emissions of polycyclic aromatic hydrocarbons in Quito, Ecuador”. In: *Environmental Pollution* 157.2, pp. 528–536. ISSN: 0269-7491. DOI: http://dx.doi.org/10.1016/j.envpol.2008.09.041. URL: http://www.sciencedirect.com/science/article/pii/S026974910800448X.

Brockmann Consult GmbH (2017). *SNAP: Scientific Image Processing Toolbox*. URL: https://web.brockmann-consult.de/portfolio/earth-scientific-image-processing/.

Brodu, Nicolas (2016). “Super-resolving multiresolution images with band-independant geometry of multispectral pixels”. In: *CoRR* abs/1609.07986. arXiv: 1609.07986. URL: http://arxiv.org/abs/1609.07986.

Calabrese, Justin M. and Fagan, William F. (2004). “A comparison-shopper’s guide to connectivity metrics”. In: *Frontiers in Ecology and the Environment* 2.10, pp. 529–536. ISSN: 1540-9309. DOI: 10.1890/1540-9295(2004)002[0529:ACGTCM]2.0.CO;2. URL: http://dx.doi.org/10.1890/1540-9295(2004)002[0529:ACGTCM]2.0.CO;2.

Clewley, Daniel, Bunting, Peter, Shepherd, James, Gillingham, Sam, Flood, Neil, Dymond, John, Lucas, Richard, Armston, John, and Moghaddam, Mahta (2014). “A Python-Based Open Source System for Geographic Object-Based Image Analysis (GEOBIA) Utilizing Raster Attribute Tables”. In: *Remote Sensing* 6.7, pp. 6111–6135. ISSN: 2072-4292. DOI: 10.3390/rs6076111. URL: http://www.mdpi.com/2072-4292/6/7/6111.

Cobo, Daniela and Neira, Carolina (2018). *Identificación de tejidos urbanos en la ciudad de Cuenca dentro del límite del área de influencia según el Plan de Ordenamiento Territorial del Cantón Cuenca (2015)*.

Congalton, Russell G. and Green, Kass (2009). *Assessing the Accuracy of Remotely Sensed Data, 2nd Edition*. CRC Press, Taylor & Francis Group, 6000 Broken Sound Parkway NW, Suite 300, Boca Raton, FL 33487-2742.

European Space Agency (ESA) (2017a). *Sentinel online - user guides*. URL: https://sentinel.esa.int/web/sentinel/missions/sentinel-2/instrument-payload/resolution-and-swath.

— (2017b). *SENTINEL-1 SAR User Guide*. URL: https://sentinels.copernicus.eu/web/sentinel/user-guides/sentinel-1-sar.

Foody, Giles M. (2009). “Sample size determination for image classification accuracy assessment and comparison”. In: *International Journal of Remote Sensing* 30.20, pp. 5273–5291. DOI: 10.1080/01431160903130937. eprint: https://doi.org/10.1080/01431160903130937. URL: https://doi.org/10.1080/01431160903130937.

Haala, Norbert and Brenner, Claus (1999). “Extraction of buildings and trees in urban environments”. In: *ISPRS Journal of Photogrammetry and Remote Sensing* 54.2, pp. 130–137. ISSN: 0924-2716. DOI: https://doi.org/10.1016/S0924-2716(99)00010-6. URL: http://www.sciencedirect.com/science/article/pii/S0924271699000106.

Hermida, M. Augusta, Orellana, Daniel, and Osorio, Pablo (2017). *REDU-FUT. Más allá del petróleo. Un estudio de la relación entre la forma urbana y el transporte en dos ciudades del Ecuador.* URL: https://llactalab.ucuenca.edu.ec/.

Huang, Xin, Zhu, Tingting, Zhang, Liangpei, and Tang, Yuqi (2014). “A novel building change index for automatic building change detection from high-resolution remote sensing imagery”. In: *Remote Sensing Letters* 5.8, pp. 713–722. DOI: 10.1080/2150704X.2014.963732. eprint: https://doi.org/10.1080/2150704X.2014.963732. URL: https://doi.org/10.1080/2150704X.2014.963732.

Inostroza, Luis, Baur, Rolf, and Csaplovics, Elmar (2013). “Urban sprawl and fragmentation in Latin America: A dynamic quantification and characterization of spatial patterns”. In: *Journal of Environmental Management* 115, pp. 87–97. ISSN: 0301-4797. DOI: http:

//dx.doi.org/10.1016/j.jenvman.2012.11.007. URL: http://www.sciencedirect.com/science/article/pii/S0301479712005920.

Instituto Nacional de Estadística y Censos (2010). *Proyección de la población ecuatoriana*. URL: http://www.ecuadorencifras.gob.ec/inec-presenta-sus-proyecciones-poblacionales-cantonales/.

Japan Aerospace Exploration Agency (2017). *ALOS Global Digital Surface Model "ALOS World 3D - 30m" (AW3D30)*. URL: http://www.eorc.jaxa.jp/ALOS/en/aw3d30/index.htm.

Kang, Chaogui, Ma, Xiujun, Tong, Daoqin, and Liu, Yu (2012). "Intra-urban human mobility patterns: An urban morphology perspective". In: *Physica A: Statistical Mechanics and its Applications* 391.4, pp. 1702–1717. ISSN: 0378-4371. DOI: http://dx.doi.org/10.1016/j.physa.2011.11.005. URL: http://www.sciencedirect.com/science/article/pii/S0378437111008405.

Kulkarni, Arun D. and Lowe, Barrett (2016). "Random Forest Algorithm for Land Cover Classification". In: *International Journal on Recent and Innovation Trends in Computing and Communication* 4.3, pp. 58–63. ISSN: 2321-8169. URL: http://www.ijritcc.org.

McFeeters, S.K. (1996). "The use of the Normalized Difference Water Index (NDWI) in the delineation of open water features". In: *International Journal of Remote Sensing* 17.7, pp. 1425–1432. DOI: 10.1080/01431169608948714. eprint: https://doi.org/10.1080/01431169608948714. URL: https://doi.org/10.1080/01431169608948714.

Ministerio de Agricultura, Ganadería, Acuacultura y Pesca (2017). *Sistema Nacional de Informacion de Tierras Rurales e Infraestructura Tecnológica*. URL: http://www.sigtierras.gob.ec.

Mueller-Wilm, U., Devignot, O., and Pessiot, L. (2018). *S2 MPC Sen2Cor Software Release Note Ref. S2-PDGS-MPC-L2A-SRN-V2.5.5*. URL: http://step.esa.int/thirdparties/sen2cor/2.5.5/docs/S2-PDGS-MPC-L2A-SRN-V2.5.5.pdf.

Ng, Edward, Yuan, Chao, Chen, Liang, Ren, Chao, and Fung, Jimmy C.H. (2011). "Improving the wind environment in high-density cities by understanding urban morphology and surface roughness: A study in Hong Kong". In: *Landscape and Urban Planning* 101.1, pp. 59–74. ISSN: 0169-2046. DOI: http://dx.doi.org/10.1016/j.landurbplan.2011.01.004. URL: http://www.sciencedirect.com/science/article/pii/S0169204611000326.

Pesaresi, Martino and Benediktsson, Jon Atli (2001). "A New Approach for the Morphological Segmentation of High-Resolution Satellite Imagery". In: *IEEE Transactions on Geoscience and Remote Sensing* 39.2, pp. 309–320.

Peteri, Renaud and Ranchin, Thierry (2004). "Multiresolution Snakes for urban road extraction from Ikonos and Quickbird images". In: *Remote Sensing in Transition*. URL: https://pdfs.semanticscholar.org/fc43/67c023b5365b9aa48ffb95baf9304a5f2bac.pdf.

Planet Lab Inc. (2017). *Planet Satellite Imagery Products*. URL: https://www.planet.com/docs/spec-sheets/sat-imagery/.

Radoux, Julien, Chomé, Guillaume, Jacques, Damien Christophe, Waldner, François, Bellemans, Nicolas, Matton, Nicolas, Lamarche, Céline, d'Andrimont, Raphaël, and De-

fourny, Pierre (2016). “Sentinel-2’s Potential for Sub-Pixel Landscape Feature Detection”. In: *Remote Sensing* 8.488. ISSN: 2072-4292. DOI: 10.3390/rs8060488. URL: http://www.mdpi.com/2072-4292/8/6/488.

Sadalla, Edward K. and Staplin, Lorin J. (1980). “The Perception of Traversed Distance”. In: *Environment and Behavior* 12.2, pp. 167–182. DOI: 10.1177/0013916580122003. URL: https://doi.org/10.1177/0013916580122003.

Small, Christopher (2002). “A global analysis of urban reflectance”. In: *International Journal of Remote Sensing* 26.4, pp. 661–681. URL: http://archive.iussp.org/Activities/wgc-urb/Small2.pdf.

Song, Yan, Popkin, Barry, and Gordon-Larsen, Penny (2013). “A national-level analysis of neighborhood form metrics”. In: *Landscape and Urban Planning* 116.Supplement C, pp. 73–85. ISSN: 0169-2046. DOI: https://doi.org/10.1016/j.landurbplan.2013.04.002. URL: http://www.sciencedirect.com/science/article/pii/S0169204613000637.

Sugg, Zachary P., Finke, Tobias, Goodrich, David C., Moran, M. Susan, and Yool, Stephen R. (2014). “Mapping Impervious Surfaces Using Object-oriented Classification in a Semiarid Urban Region”. In: *Photogrammetric Engineering & Remote Sensing* 80.4, pp. 343–352. DOI: 10.14358/PERS.80.4.343. URL: https://pdfs.semanticscholar.org/f847/ee0dd42c0f4efd0c7dea0afeee26834689fc.pdf.

U.S. Department of the Interior - U.S. Geological Survey (2017). *USGS Spectral Library*. URL: speclab.cr.usgs.gov/spectral-lib.html.

Vernez-Moudon, Anne (1997). “Urban morphology as an emerging interdisciplinary field”. In: *Urban Morphology*. Vol. 1, pp. 3–10. URL: http://urbanmorphology.org/pdf/moudon1997.pdf.

Wang, Weixing, Yang, Nan, Zhang, Yi, Wang, Fengping, Cao, Ting, and Eklund, Patrik (2016). “A review of road extraction from remote sensing images”. In: *Journal of Traffic and Transportation Engineering (English Edition)* 3.3, pp. 271–282. ISSN: 2095-7564. DOI: https://doi.org/10.1016/j.jtte.2016.05.005. URL: http://www.sciencedirect.com/science/article/pii/S2095756416301076.

Waqar, Mirza Muhammad, Mirza, Johum Fatimah, Mumtaz, Rafia, and Hussain, Ejaz (2012). “Development of New Indices for Extraction of Built-Up Area and Bare Soil from Landsat Data.” In: *Open Access Scientific Reports* 1.136. DOI: 10.4172/scientificreports.13.

Weng, Qihao (2012). “Remote sensing of impervious surfaces in the urban areas: Requirements, methods, and trends”. In: *Remote Sensing of Environment* 117. Remote Sensing of Urban Environments, pp. 34–49. ISSN: 0034-4257. DOI: http://dx.doi.org/10.1016/j.rse.2011.02.030. URL: http://www.sciencedirect.com/science/article/pii/S0034425711002811.

Wentz, Elizabeth A. (2000). “A Shape Definition for Geographic Applications Based on Edge, Elongation, and Perforation”. In: *Geographical Analysis* 32.1, pp. 95–112. URL: http://onlinelibrary.wiley.com/doi/10.1111/j.1538-4632.2000.tb00419.x/pdf.

Wheeler, Stephen M. (2015). “Built Landscapes of Metropolitan Regions: An International Typology”. In: *Journal of the American Planning Association* 81.3, pp. 167–190. DOI: 10.1080/01944363.2015.1081567. URL: http://dx.doi.org/10.1080/01944363.2015.1081567.